De novo variants in *PLCG1* are associated with hearing impairment, ocular pathology, and cardiac defects

Mengqi Ma,[1,2,*] Yiming Zheng,[1,2,12,*] Shenzhao Lu,[1,2] Xueyang Pan,[1,2] Kim C. Worley,[1] Lindsay C. Burrage,[1] Lauren S. Blieden,[1] Aimee Allworth,[3] Wei-Liang Chen,[3,13] Giuseppe Merla,[4,5] Barbara Mandriani,[6] Jill A. Rosenfeld,[1] David Li-Kroeger,[7] Debdeep Dutta,[1,2] Shinya Yamamoto,[1,2] Michael F. Wangler,[1,2] Undiagnosed Diseases Network, Ian A. Glass,[3,8,9] Sam Strohbehn,[3] Elizabeth Blue,[3,9,10] Paolo Prontera,[11] Seema R. Lalani,[1] Hugo J. Bellen,[1,2,#]

Affiliations:

1. Department of Molecular and Human Genetics, Baylor College of Medicine, Houston, TX 77030, USA
2. Jan and Dan Duncan Neurological Research Institute at Texas Children's Hospital, Houston, TX 77030, USA
3. Division of Medical Genetics, Department of Medicine, University of Washington School of Medicine, Seattle, WA 98195, USA
4. Laboratory of Regulatory & Functional Genomics, Fondazione IRCCS Casa Sollievo della Sofferenza, San Giovanni Rotondo, Foggia 71013, Italy
5. Department of Molecular Medicine & Medical Biotechnology, University of Naples Federico II, Naples 80131, Italy
6. Department of Interdisciplinary Medicine, University of Bari "Aldo Moro", Bari 70121, Italy
7. Department of Neurology, Baylor College of Medicine, Houston, TX 77030, USA
8. Division of Genetic Medicine, Department of Pediatrics, University of Washington School of Medicine, Seattle, WA 98195, USA

9. Brotman Baty Institute, Seattle, WA 98195, USA

10. Institute for Public Health Genetics, University of Washington, Seattle, WA 98195, USA

11. Medical Genetics Unit, Hospital of Perugia, Perugia 06129, Italy

12. Current affiliation: State Key Laboratory of Cellular Stress Biology, School of Life Sciences, Faculty of Medicine and Life Sciences, Xiamen University, Xiamen 361102, China

13. Current affiliation: Children's National Medical Center and George Washington University, Washington DC 20010, USA

* These authors contributed equally

Correspondence: Hugo J. Bellen: hbellen@bcm.edu

Abstract

Phospholipase C isozymes (PLCs) hydrolyze phosphatidylinositol 4,5-bisphosphate into inositol 1,4,5-trisphosphate and diacylglycerol, important signaling molecules involved in many cellular processes. *PLCG1* encodes the PLCγ1 isozyme that is broadly expressed. Hyperactive somatic mutations of *PLCG1* are observed in multiple cancers, but only one germline variant has been reported. Here we describe three unrelated individuals with *de novo* heterozygous missense variants in *PLCG1* (p.Asp1019Gly, p.His380Arg, and p.Asp1165Gly) who exhibit variable phenotypes including hearing loss, ocular pathology and cardiac septal defects. To model these variants *in vivo*, we generated the analogous variants in the *Drosophila* ortholog, *small wing* (*sl*). We created a null allele sl^{T2A} and assessed the expression pattern. *sl* is broadly expressed, including in wing discs, eye discs, and a subset of neurons and glia. Loss of *sl* causes wing size reductions, ectopic wing veins and supernumerary photoreceptors. We document that mutant flies exhibit a reduced lifespan and age-dependent locomotor defects. Expressing wild-type *sl* in sl^{T2A} mutant rescues the loss-of-function phenotypes whereas expressing the variants causes lethality. Ubiquitous overexpression of the variants also reduces viability, suggesting that the variants are toxic. Ectopic expression of an established hyperactive *PLCG1* variant (p.Asp1165His) in the wing pouch causes severe wing phenotypes, resembling those observed with overexpression of the p.Asp1019Gly or p.Asp1165Gly variants, further arguing that these two are gain-of-function variants. However, the wing phenotypes associated with p.His380Arg overexpression are mild. Our data suggest that the *PLCG1 de novo* heterozygous missense variants are pathogenic and contribute to the features observed in the probands.

Keywords: Phospholipase C; *Drosophila*; phenotypic heterogeneity; *PLCG1* gain-of-function variants

Introduction

The inositol lipid-specific phospholipase C (PLC) isozymes are key signaling proteins that play critical roles in transducing signals from hormones, growth factors, neurotransmitters, and many extracellular stimuli [1-3]. The PLCs selectively hydrolyze phosphatidylinositol 4,5-bisphosphate (PIP2) into inositol 1,4,5-trisphosphate (IP3) and diacylglycerol (DAG) [4,5]. PIP2 functions as a membrane anchor for numerous proteins and affects membrane dynamics and ion transport [6-8]. The two products, IP3 and DAG, are important intracellular second messengers involved in Ca^{2+} signaling regulation and protein kinase C signaling activation, respectively [9,10]. Hence, PLC orchestrates diverse cellular processes and behaviors, including cell growth, differentiation, migration, and cell death [11-14]. There are at least thirteen PLC isozymes grouped in 6 classes (β, δ, ε, γ, η, ζ) in mammals with similar enzymatic function, but each PLC has its own spectrum of activators, expression pattern, and subcellular distribution [15-17].

PLCG1 [MIM: 172420] encodes the PLCγ1 isozyme. PLCγ1 is directly activated by receptor tyrosine kinases (RTKs) as well as cytosolic receptors coupled to tyrosine kinases [18]. Upon tyrosine phosphorylation, PLCγ1 undergos conformational changes that release its autoinhibition upon which it associates with the plasma membrane to bind and hydrolyze its substrates [19-21]. There is a second PLCγ isozyme, PLCγ2, encoded by *PLCG2* [MIM: 600220]. Although these two isozymes have similar protein structure and activation mechanism, they are differentially expressed and regulated, and play non-redundant roles [22,23]. *PLCG2* is mostly expressed in cells of the hematopoietic system and mainly functions in immune response, causing human diseases associated with immune disorders [24-27]. However, *PLCG1* is ubiquitously expressed and is enriched in the central nervous system (CNS) [28]. *Plcg1* is essential in mice, and a null allele causes embryonic lethality with developmental defects in the vascular, neuronal, and immune system [29,30]. *PLCG1* has emerged as a possible driver for cell proliferation, and increased expression level of *PLCG1* has been observed in breast cancer, colon cancer, and squamous cell carcinoma [31-34]. Moreover, hyperactive somatic mutations of *PLCG1* have been observed in

angiosarcomas and T cell leukemia/lymphomas [35-37]. However, the genotype-phenotype association of germline *PLCG1* variants has yet to be explored.

Results

Individuals with *de novo* heterozygous missense variants in *PLCG1* exhibit hearing impairment, ocular pathology, and cardiac defects

Here, we report three unrelated individuals with *de novo* heterozygous missense variants in *PLCG1* (GenBank: NM_002660.3). Proband 1 (c.3056A>G, p.Asp1019Gly) and proband 2 (c.1139A>G, p.His380Arg) were identified through the Undiagnosed Diseases Network (UDN) [45] and proband 3 (c.3494A>G, p.Asp1165Gly) was identified via GeneMatcher [46]. The probands range in age from 5 years to 20 years. The phenotypes of the probands partially overlap but show a diverse spectrum. Pertinent shared features include deafness (probands 1 and 3), ophthalmologic abnormalities (probands 1 and 2), and cardiac septal defects (probands 1 and 3). Two of the three individuals show abnormal brain MRI (probands 1 and 2), and one has immune defects (proband 3). Additional variants identified in the probands are discussed in supplemental data. **[*As per medRxiv policy, the whole and detailed case history for the probands have been removed. To obtain more detailed information, please contact the authors*]**

The proband-associated missense *PLCG1* variants are located in conserved protein domains and are predicted to be deleterious

PLCG1 is predicted to be tolerant to loss-of-function alleles with a pLI score [47] of 0.16, suggesting that loss of one copy of the gene is unlikely to cause haploinsufficiency in humans and consistent with the presence of many protein truncating variants in gnomAD [48]. However, the missense constraint Z score [47]

of *PLCG1* is 3.69, suggesting it is intolerant to missense variants. In addition, the prediction based on the DOMINO algorithm indicates that *PLCG1* variants are likely to be dominant [49]. The *in-silico* pathogenicity predictions suggest that these variants are likely to be pathogenic (Table S1) based on MARRVEL [50].

The three variants identified from the probands map to different conserved domains of PLCγ1, and each variant affects an amino acid residue that is conserved from flies to humans (Figure 1A and Figure 1B). The p.Asp1019Gly and p.His380Arg variants map to the catalytic core domains, and the p.Asp1165Gly is in the C-terminal C2 domain. PLCγ1 contains other conserved domains including an N-terminal pleckstrin homology (PH) domain, four EF hand motifs, as well as a PLCγ-specific regulatory array that is composed of a split PH domain (sPH), two Src homology 2 (nSH2 and cSH2) domains and a Src homology 3 (SH3) domain.

small wing (*sl*) is the fly ortholog of human *PLCG1*

To obtain information about the nature of the proband-associated variants, we utilize *Drosophila* to model the variants *in vivo*. Flies have three genes encoding PLC isozymes (Table S2). Among them, *small wing* (*sl*) is predicted to be the ortholog of *PLCG1* with a DIOPT (DRSC Integrative Ortholog Prediction Tool) score of 17/18 (DIOPT version 9.0) [51]. The encoded proteins share 39% identity and 57% similarity and are composed of similar conserved domains (Figure 1A). *sl* is also predicted to be the ortholog of *PLCG2* with a DIOPT score of 12/18. These data suggest that *sl* corresponds to two human genes encoding the PLCγ isozymes. We generated transgenic flies carrying the *UAS-human PLCG1* cDNAs for both the reference (*UAS-PLCG1*^{Reference}) and the variants (*UAS-PLCG1*^{D1019G}, *UAS-PLCG1*^{H380R}, and *UAS-PLCG1*^{D1165G}). Given the high level of protein sequence homology and the conservation of the affected amino acids (Figure 1B), we also generated transgenic flies for the reference and analogous variants in the fly *sl* cDNA, namely *UAS-sl*^{WT} and *UAS-sl*^{variants} (*UAS-sl*^{D1041G}, *UAS-sl*^{H384R}, and *UAS-sl*^{D1184G}).

sl is on the X chromosome, and several alleles of *sl* have been isolated or generated previously, including sl^{2}, sl^{KO} and sl^{T2A} (Figure 1C). sl^{2} carries a 13bp deletion in the third exon that leads to a frameshift and early stop gain [52]. sl^{2} is a strong loss-of-function allele that causes small wing size, ectopic wing veins and extra R7 photoreceptors [52]. sl^{KO} was generated by CRISPR-mediated genomic editing that removes nearly the entire gene [53]. sl^{T2A} allele was generated by inserting an FRT-SA-T2A-GAL4-polyA-FRT cassette as an artificial exon into the first coding intron of *sl* (Figure 1C) [54,55]. The polyA arrests transcription, and sl^{T2A} is a strong loss-of-function allele (Figure S1A). The T2A viral sequence triggers ribosomal skipping and leads to the production of GAL4 proteins [56,57] that are expressed in the proper spatial and temporal pattern of *sl*. This allows us to assess the expression pattern of *sl* by driving the expression of a *UAS-fluorescent protein* [54], or to assess the function of variants by expressing the human *UAS-reference/variant cDNAs* [42,58-62]. In addition, the cassette is flanked by two FRT sites so that it can be excised from the cells that express the gene in the presence of *UAS-Flippase* and revert the mutant phenotypes (Figure 1C) [54].

We first assessed the expression pattern of *sl* by driving *UAS-mCherry.nls* (an mCherry that localizes to nuclei) with sl^{T2A}. *sl* is expressed in the 3rd larval wing discs and eye discs (Figure 2A), consistent with the loss-of-function phenotypes observed in the wings and eyes [52]. The expression pattern of *sl* in the wing discs is not homogenous. Higher expression levels are observed in the anterior compartment and along both the anterior/posterior and dorsal/ventral compartment boundaries (Figure 2A). The hemizygous sl^{T2A}/Y male flies and the trans-heterozygous sl^{T2A}/sl^{2} or sl^{T2A}/sl^{KO} female flies show reduced wing size and ectopic wing veins (Figure 2B and Figure S1B), as well as additional photoreceptors in the eye (Figure 2C and Figure S1C). These phenotypes can be rescued by *UAS-Flippase* or by introducing a genomic rescue construct (*Dp(1;3)DC313* [63], Figure 1C) that covers the *sl* locus (Figure 2B and Figure 2C). These data show that all the observed phenotypes in sl^{T2A} mutants can be attributed to the loss of *sl*.

_sl_ is expressed in the fly CNS and loss of _sl_ causes longevity and locomotion defects

Given that human *PLCG1* is highly expressed in the central nervous system (CNS) [28] and that the probands present with neurologic phenotypes including hearing or vision deficits (Table 1), we investigated the expression pattern and the cell type specificity of *sl* in the CNS of flies. *sl* is expressed in the larval CNS as well as the adult brain, and co-staining with the pan-neuronal marker Elav [64] and glial marker Repo [65] show that *sl* is expressed in a subset of neurons and glia cells in the CNS (Figure 3A). We therefore assessed the longevity and climbing of sl^{T2A} flies. Compared to the wild-type w^{1118} flies, sl^{T2A}/Y hemizygous mutant flies show a shortened lifespan and a progressively reduced climbing ability. These phenotypes can be rescued by expression of the wild-type *sl* cDNA (sl^{T2A}/Y; *UAS-*sl^{WT}) (Figure 3B).

Functional assays in flies indicate that the *PLCG1* variants are toxic

To assess the impact of the variants, we expressed the *sl* variant cDNAs in the sl^{T2A}/Y hemizygous mutant males (sl^{T2A}/Y; *UAS-*$sl^{variants}$) and compared their rescue ability with the wild-type *sl* (sl^{T2A}/Y; *UAS-*sl^{WT}). As shown in Figure 4A, the sl^{T2A}/Y mutant flies (or the ones expressing a *UAS-Empty* control construct) have a slightly reduced eclosion rate but expression of the sl^{WT} cDNA fully rescues the percentage of eclosing progeny as measured by the Mendelian ratio. In contrast, expressing sl^{H384R} causes a severe reduction of the number of eclosing flies with very few escapers (sl^{T2A}/Y; *UAS-*sl^{H384R}). Moreover, expression of the sl^{D1041G} or sl^{D1184G} leads to 100% lethality (Figure 4A). These data clearly indicate that the three variants are toxic.

Given that the expression of these *sl* cDNAs is performed in a null mutant background, we opted to assess the phenotypes associated with ectopic expression assays by overexpressing the wild-type or variant *sl* cDNAs using a strong ubiquitous driver, *Tub-GAL4*. Overexpression of sl^{WT} shows no impact on viability. However, overexpression of sl^{H384R} leads to ~36% lethality, while overexpression of sl^{D1041G} or sl^{D1184G} results in 100% lethality at the L1-L2 larval stage (Figure 4B). Hence, ubiquitous overexpression assays cause similar but less severe lethal phenotypes than the expression assays driven by sl^{T2A}. This difference

may arise from the different expression patterns and levels of *Tub-GAL4* and sl^{T2A}. Importantly, sl^{T2A} drives expression in the cells that normally express *sl*. In summary, the data argue that the *sl* variants are likely to be gain-of-function or neomorphic alleles and that sl^{D1041G} and sl^{D1184G} are very strong toxic alleles whereas sl^{H384R} is a milder allele.

To compare the *sl* and *PLCG1* associated phenotypes, we conducted similar assays using human *PLCG1* cDNAs. Expression of $PLCG1^{Reference}$ in the sl^{T2A}/Y mutant flies (sl^{T2A}/Y; *UAS-*$PLCG1^{Reference}$) (Figure 4A) reduces viability by 90%, while the ubiquitous expression of $PLCG1^{Reference}$ under the control of *Tub-GAL4* (*Tub-GAL4 > UAS-*$PLCG1^{Reference}$) reduces viability by 63% (Figure 4B). These data argue that the reference human *PLCG1* cDNA is toxic in flies. Expression of $PLCG1^{H380R}$ in the sl^{T2A}/Y mutant flies (sl^{T2A}/Y; *UAS-*$PLCG1^{H380R}$) leads to a modest increase in lethality when compared to $PLCG1^{Reference}$ (Figure 4A), whereas *Tub-GAL4 > UAS-*$PLCG1^{H380R}$ is not worse than $PLCG1^{Reference}$ (Figure 4B). In contrast, expression of $PLCG1^{D1019G}$ or $PLCG1^{D1165G}$ results in 100% lethality using either of the drivers (Figure 4A and 4B). In summary, expressing the human *PLCG1* in flies induces toxicity, and $PLCG1^{H380R}$ has only slightly increased toxicity when compared to $PLCG1^{Reference}$. However, the $PLCG1^{D1019G}$ or $PLCG1^{D1165G}$ variants display a severe gain of toxicity.

Since overexpressing fly sl^{WT} does not cause viability issues (Figure 4B), the observed toxicity associated with $PLCG1^{Reference}$ in flies may be due to the elevated expression of the human proteins. This hypothesis can be assessed by ectopic expression assays performed by raising the flies at different temperatures. The GAL4-UAS system is highly temperature-dependent since the promoter in the UAS construct contains an Hsp-70 promoter [66]: at 29°C the expression level is much higher than at 25°C, and at 22°C the expression level is significantly lower than at 25°C [67]. As shown in Figure 4C, the *Tub-GAL4>UAS-*$PLCG1^{Reference}$ flies exhibit a high lethality ratio when raised at 29°C (~63% lethal). This lethality ratio decreased to ~43% when the flies are raised at 25°C whereas the flies are viable at 22°C. This shows that the toxicity is highly dependent on protein levels. Indeed, the expression levels can be further lowered by using a weak ubiquitous GAL4 driver, *da-GAL4*. The *da-GAL4 > UAS-*$PLCG1^{Reference}$ or *UAS-*$PLCG1^{H380R}$ flies are

viable at the three tested temperatures (29°C, 25°C, and 22°C). In contrast, *da-GAL4* > *UAS-PLCG1*^{D1019G} or *UAS-PLCG1*^{D1165G} flies are lethal at 29°C, semi-lethal (~80%-85% lethal) at 25°C, and viable at 22°C (Figure 4C, right panel). The animals that escape lethality at 25°C have smaller pupae (Figure S2) and a reduced adult body size, showing that growth is impeded. In summary, these data consistently confirmed that ubiquitous elevated expression levels of the human *PLCG1* is toxic in flies.

To assess other phenotypes, we used *nub-GAL4* to mostly drive the expression of *UAS-PLCG1* or *UAS-sl* cDNAs in the wing disc, a well-established model to study growth and differentiation in a tissue that is dispensable for viability [68]. Overexpression of either *PLCG1*^{Reference} or *sl*^{WT} in the wing disc leads to slightly smaller wings with a ~10% reduction in size when compared to expressing the *UAS-Empty* control (Figure S3). Hence, both loss and overexpression of *sl* in the wing lead to a size reduction (Figure 2B and S3). This implies a potential dosage-dependent regulation on wing growth by the PLCγ isozymes, although the underlying mechanism is unknown. Overexpression of the *PLCG1*^{H380R} or *sl*^{H384R} in the wing results in ~5% reduction in wing size when compared to the *PLCG1*^{Reference} or *sl*^{WT} (Figure S3). However, overexpression of *PLCG1*^{D1019G} or *PLCG1*^{D1165G} results in severe wing phenotypes characterized by notched wing margins, fused/thickened veins and reduced wing sizes (Figure 5A). Notably, overexpressing fly *sl*^{D1041G} leads to very similar morphological defects as the corresponding human *PLCG1*^{D1019G} variant, indicating that the observed wing phenotypes are indeed due to alterations in *PLCG1/sl* functions. These data also argue that the human *PLCG1* functions in the same pathways as *sl*. Furthermore, overexpressing the *sl*^{D1184G} leads to pupal lethality (Figure 5A). This suggests that this variant has a more severe impact on development than the other variants and is not inconsistent with the observation that *nub-GAL4* drives some expression of *UAS-cDNA* in the nervous system as well [69].

We also assessed the effect of ectopic expression of human *PLCG1* on eye development using an eye-specific driver *eyeless-GAL4* (*ey-GAL4*). The expression of *PLCG1*^{Reference} or *PLCG1*^{H380R} in fly eyes leads to a mild reduction in eye size, while the expression of *PLCG1*^{D1019G} or *PLCG1*^{D1165G} leads to a severe reduction in eye size (Figure S4). In summary, the eye data are consistent with the wing data, showing

that *PLCG1*^{D1019G} and *PLCG1*^{D1165G} are more toxic than *PLCG1*^{Reference}. On the other hand, the toxicity of *PLCG1*^{H380R} is milder and can be distinguished from that of the *PLCG1*^{Reference} only in certain contexts.

The p.Asp1019Gly and p.Asp1165Gly variants are gain-of-function variants

Previous studies have identified a very strong gain-of-function somatic *PLCG1* variant p.Asp1165His in adult T cell leukemia/lymphoma [20,70,71]. This variant has been documented to cause a very dramatic increase in phospholipase activity *in vitro* [20,71]. To characterize the impact of this hyperactive variant *in vivo*, we generated transgenic flies with this variant and tested *PLCG1*^{D1165H} in our tissue-specific expression assays. Overexpression of *PLCG1*^{D1165H} in the eye using *ey-GAL4* causes lethality at 29°C (Figure S4), arguing that it is highly toxic. As shown in Figure 5B, overexpressing *PLCG1*^{D1165H} in the wing using the *nub-GAL4* driver causes lethality at 29°C. However, these flies survive when they are raised at 25°C, yet the wings show severe morphological defects, including notched wing margins, thickened veins as well as reduced wing size. These phenotypes are similar to, but more severe than, the defects observed in the wings overexpressing *PLCG1*^{D1019G} or *PLCG1*^{D1165G} (Figure 5B). These data provide compelling evidence that these two variants are gain-of-function variants.

Discussion

A recent study reported an individual with a *de novo* heterozygous gain-of-function germline variant in *PLCG1*, p.Ser1021Phe [72]. The proband exhibited an early-onset and severe immune dysregulation with autoimmune and autoinflammatory symptoms. Tao *et al*. performed *in vitro* and *ex vivo* experiments using cultured cell lines transfected with *PLCG1* constructs and peripheral blood mononuclear cells from the proband, respectively. They showed that the p.Ser1021Phe variant led to a 1.5-2 fold increase in intracellular IP3 production compared to controls. However, in our *in vivo* assays, overexpression of *PLCG1*^{S1021F} in wings or eyes does not cause obvious phenotypes when compared to *PLCG1*^{Reference}

(Figure S5), which is clearly distinct from the other gain-of-function variants tested in our assays (p.Asp1019Gly, p.Asp1165Gly and p.Asp1165His) (Figure 5B). It is notable that the three probands reported here are discordant for immune-related phenotypes. Proband 1 with the p.Asp1019Gly variant has no immune dysregulation symptoms. Proband 2 with the p.His380Arg variant has a relapsing steroid responsive inflammatory encephalomyelitis, which is very different from the autoimmune symptoms reported by Tao *et al* [72]. Finally, proband 3 with the p.Asp1165Gly variant presents with a T cell lymphocytopenia with recurrent infections suggesting that the individual is immune compromised. Hence, the immune phenotypes in the individuals reported here are very heterogeneous or absent, and inconsistent with an autoimmune disease. In summary, the immune-related phenotypes and their association with *PLCG1* variants will need to be explored in more depth.

Previously, studies based on biochemical assays and protein structures provided insights into how the variants studied here may affect the enzymatic activity of PLCγ1 (the established protein structure of full-length rat Plcg1 is shown in Figure 6A). In its basal state, the PLCγ-specific regulatory array (sPH-nSH2-cSH2-SH3) forms autoinhibitory interfaces with the catalytic domains. Upon activation by the RTKs through binding to nSH2, PLCγ1 is phosphorylated, which in turn induces the dissociation of the inhibitory cSH2 domain from the C2 domain. This triggers conformational rearrangements, allowing the enzyme to associate with the membrane and exposing the catalytic domains to allow hydrolysis of PIP2 [19-21,73,74]. As shown in Figure 6A, the location of the three variants modeled in this study (Asp1019Gly, His380Arg and Asp1165Gly) are either within the catalytic domains or at the intramolecular interfaces. The p.Asp1019Gly and p.Asp1165Gly variants impact crucial residues involved in autoinhibition. Specifically, the p.Asp1019Gly variant affects a residue located at the apex of the hydrophobic ridge within the Y box (Figure 6B), which is important for the interaction between the sPH domain and the Y box. This interaction is critical for the autoinhibition by blocking the membrane engagement of the catalytic core domain prior to enzymatic activation [20,75]. Notably, substitution of Asp1019 with Lys (D1019K) has been demonstrated to enhance basal phospholipase activity by approximately 15 fold *in*

vitro [76]. Similarly, another hotspot somatic variant, p.Ser345Phe, located at the hydrophobic ridge within the X box, involved in the interaction between the sPH domain and X box, has also been verified to be hyperactive [37,77]. In contrast, the p.Ser1021Phe variant described by Tao *et al.* [72] lies outside the hydrophobic ridge of the interface between the sPH domain and Y box (Figure 6B). On the other hand, the p.Asp1165Gly variant affects a residue situated within a loop of the C2 domain (Figure 6C). The Asp1165 residue plays a key role in stabilizing the interaction between the cSH2 domain and the C2 domain to maintain the autoinhibited state [78]. As mentioned above, the somatic variant p.Asp1165His leads to significantly elevated phospholipase activity *in vitro* [71,73], and results in severe phenotypes *in vivo* (Figure 5B). In contrast, the p.His380Arg variant impacts the His380 residue within the X box, situated near the bound Ca^{2+} cofactor in the catalytic core (Figure 6D). His380 plays a role in coordination of phosphate 1 of IP3 [74]. While this residue may not be key to the autoinhibition, it is important to the phospholipase activity. Substitution of His380 with Phe or Ala (H380F, H380A) has been reported to suppress PIP2 hydrolysis and IP3 production [79,80]. Substitution of the His380 with Arg in p.His380Arg variant may create a more basic environment, impacting the lipase activity in a distinct way. Our *in vivo* data are consistent with the published *in vitro* data, strengthening our conclusion that the variants are pathogenic and impact the protein function.

In summary, we report three individuals with *de novo* heterozygous missense variants in *PLCG1* presenting with disease features that encompass ophthalmologic, hearing, and cardiac defects with variable expressivity. Our functional assays provide compelling *in vivo* evidence that the *PLCG1* variants alter normal protein function. However, additional genetic variants (see Table 1) and environmental factors may contribute to some of the diverse phenotypes observed in these three individuals. Moreover, the PLCγ1 isozyme is an integral component of multiple signaling pathways, and the outcomes of its dysregulation are expected to be context dependent. Hence, different variants of *PLCG1* may impact diverse cellular processes in different tissues and cells, leading to a range of pathological changes. Even when the affected residues are in close proximity to each other, their impact on protein function can be

different [73]. Moreover, given that the p.Asp1019Gly and p.Asp1165Gly variants are hyperactive, potential therapeutic targets include specific inhibitors of PLCG1, such as antisense approaches that target the altered nucleotides [81,82].

Data and code availability

This study did not generate datasets. All reagents developed in this study are available upon request.

Conflict of Interest Statement

The Department of Molecular and Human Genetics at Baylor College of Medicine receives revenue from clinical genetic testing completed at Baylor Genetics Laboratories.

Acknowledgments

We thank the probands and families for their participation in this study. We thank Ms. Hongling Pan for transgenic fly lines. We thank Dr. Meisheng Ma for suggestions about protein structure interpretation. We thank the Bloomington Drosophila Stock Center (BDSC) for providing stocks.

Funding Statement

This work was supported by the Huffington Foundation; the Jan and Dan Duncan Neurological Research Institute at Texas Children's Hospital, and the Undiagnosed Diseases Network funded by grants from the National Institutes of Health (U01 HG010233, U01 NS134355, U01 HG007709, U01 HG007942). Sequence data analysis was supported by the University of Washington Center for Rare Disease Research (UW-CRDR; U01 HG011744, UM1 HG006493, U24 HG011746). The content is solely the responsibility

of the authors and does not necessarily represent the official views of the National Institutes of Health. H.J.B. receives support from the NIH Common Fund through the Office of Strategic Coordination/Office of the NIH Director and the NINDS (U54 NS093793) as well as ORIP (R24 OD022005 and R24 OD031447). Confocal microscopy was performed in the BCM IDDRC Neurovisualization Core, supported by the NICHD (U54 HD083092).

Author contributions

Conceptualization: M.M., Y.Z., S.R.L., I.A.G., P.P., H.J.B.; Data curation: M.M., Y.Z., S.R.L., I.A.G., E.B., P.P., H.J.B.; Formal analysis: M.M., Y.Z., S.L., J.A.R., A.A.; Funding acquisition: UDN, H.J.B.; Investigation: M.M., Y.Z., S.L.; Resources: M.M., Y.Z., W.K.C., B.L.C., B.L.S., M.G., M.B., S.Y., M.F.W., S.R.L., I.A.G., P.P., H.J.B.; Supervision: H.J.B.; Visualization: M.M., Y.Z. S.L., X.P.; Writing-original draft: M.M., Y.Z.; Writing-review & editing: M.M., Y.Z., X.P., S.L., L.D., D.D., J.A.R., S.S., W-L.C., E.B., S.R.L., I.A.G., P.P., H.J.B..

Figures and Figure Legends

Figure 1. The *PLCG1* homolog, *sl* is conserved in *Drosophila*

(A) Schematic of human PLCG1 and fly Sl protein domains and positions of the variants identified in the probands. Domain prediction is based on annotation from NCBI. Alignment of human PLCG1 and the homologous proteins. The variants are marked with boxes.

(B) All the variants affect conserved amino acids (labeled in red). Isoforms for alignment: Human PLCG1 NP_877963.1; Mouse Plcg1 NP_067255.2; Zebrafish plcg1 NP_919388.1; Fly sl NP_476726.2.

(C) Schematic of fly *sl* genomic span, transcript, alleles and the 92kb genomic rescue (GR) construct. Loss-of-function alleles of *sl* including sl^{2} (13bp deletion [52]), sl^{KO} (CRISPR-mediated deletion of the gene span [53]), and sl^{T2A} (T2A cassette inserted in the first intron, [54]) are indicated. The T2A cassette in sl^{T2A} is flanked by FRT sites and can be excised by Flippase to revert loss-of-function phenotypes. GAL4 expression in sl^{T2A} under the control by *sl* endogenous promoter can be used to assess *sl* gene expression pattern by crossing with a *UAS-mCherry.nls* reporter line, or be used to model patient variants *in vivo* by crossing with human *PLCG1* cDNAs or corresponding fly *sl* cDNAs. The primer pair used for real-time PCR is indicated.

Figure 2. sl^{T2A} is a loss-of-function allele causing phenotypes in wing and eye

(A) *sl* expression in wing and eye. Expression of *UAS-mcherry.nls* (red) was driven by sl^{T2A} to label the nuclei of the cells that expressed *sl*. *sl* is expressed in the 3rd instar larval wing disc (left) and eye disc (right). Higher magnification image of the wing disc pouch region indicated by dashed rectangle is shown. The posterior/anterior and dorsal/ventral compartment boundaries are indicated by dashed lines in yellow. Scale bars, 100μm

(B) sl^{T2A} causes wing size reduction and ectopic veins (arrowhead) in hemizygous mutant male flies. The wing phenotypes can be rescued by introduction of a genomic rescue (GR) construct or the

expression of Flippase. Scale bars, 0.5mm. The quantification of adult wing size is shown in the right panel. Each dot represents the measurement of one adult wing sample. Unpaired t test, ****p < 0.0001, mean ± SEM.

(C) sl^{T2A} causes extra photoreceptors (arrows) in the hemizygous mutant flies. The eye phenotype can be rescued by introduction of a genomic rescue (GR) construct. The photoreceptor rhabdomeres stain positive for phalloidin labeling F-actin. Scale bars, 10μm. The quantification is shown in the right panel. Each dot represents the measurement of one retina sample. Unpaired t test, ****p < 0.0001, mean ± SEM.

Figure 3. *sl* is expressed in a subset of neurons and glia in the CNS, and loss of *sl* causes behavioral defects

(A) Expression pattern of *sl* in the central nervous system observed by sl^{T2A}-driven expression of *UAS-mCherry.nls* reporter (red). In either larval or adult brain, *sl* is expressed in a subset of fly neurons and glia, which were labeled by pan-neuronal marker Elav (green, upper panel) and pan-glia marker Repo (green, lower panel). Higher magnification images of the regions indicated by dashed rectangles are shown. Scale bars, 20μm in the magnified images, 50μm in other images.

(B) Loss of *sl* causes behavioral defects in longevity and locomotion. sl^{T2A} hemizygous flies have a shorter lifespan than w^{1118} control flies. The median life span of sl^{T2A} and w^{1118} flies is 40 days and 62 days respectively. The short lifespan in sl^{T2A} flies can be rescued by a UAS transgene that expresses wild-type *sl* cDNA (sl^{WT}). Fly locomotion ability was assessed by climbing assay (see methods). sl^{T2A} flies at the age of 7 days show reduced locomotion ability and become almost immotile at the age of 35 days. The reduced locomotion ability in sl^{T2A} flies can be fully rescued by sl^{WT}. For lifespan assay, Longrank test, ****p<0.0001. For climbing assay, each dots represents one vial containing 18-22 flies for test. Unpaired t test, ****p<0.0001.

Figure 4. The variant cDNAs are toxic

(A) Summary of the viability of expressing *sl* or *PLCG1* cDNAs in sl^{T2A} mutant flies. Cross strategy: heterozygous sl^{T2A} female flies were crossed to male flies carrying *UAS-cDNAs* or control (*UAS-Empty*) constructs ,or crossed to the *y w* males as an extra control. The percentages of the hemizygous sl^{T2A} male progeny expressing different *UAS-cDNA* constructs were calculated. The expected Mendelian ratio is 0.25 (indicated by the green line in the graph). The dark gray columns represent human cDNAs, the light gray columns represent fly cDNAs, and the clear columns represent controls (*y w* or *UAS-Empty*). Each dot represents one independent replicate. Unpaired t test, *p<0.05, ****p < 0.0001, mean ± SEM.

(B) Summary of the viability of ubiquitous overexpression of *sl* or *PLCG1* cDNAs driven by *Tub-GAL4*. Expression of wild-type fly *sl* cDNA shows no impact on viability whereas expression of the *sl* variants reduces viability. Expressing human *PLCG1* cDNAs at 29°C is toxic in flies. Expression of $PLCG1^{Reference}$ or $PLCG1^{H380R}$ causes semi-lethality, whereas expression of $PLCG1^{D1019G}$ or $PLCG1^{D1165G}$ is 100% lethal at early larval stage.

(C) Summary of the viability of ubiquitous overexpression *PLCG1* cDNAs using a strong driver *Tub-GAL4* (left panel) or a weaker driver *da-GAL4* (right panel) at different temperatures. The expression level rises with higher temperatures and decreases with lower temperatures, and the toxic impact on viability correlates with the expression level. Expression of $PLCG1^{D1019G}$ or $PLCG1^{D1165G}$ causes more severe toxicity than expression of $PLCG1^{Reference}$ or $PLCG1^{H380R}$.

Figure 5. The *PLCG1* p.Asp1019Gly and p.Asp1165Gly variants are likely to be gain-of-function alleles

(A) Wing-specific overexpression of $PLCG1^{D1019G}$ or $PLCG1^{D1165G}$ causes severe wing morphology defects including notched margin (arrows) and fused/thickened veins (arrowheads), fully penetrant (the penetration ratio is indicated). Note that overexpression of the fly sl^{D1041G} (corresponding to the human $PLCG1^{D1019G}$) shows similar phenotypes. Scale bars, 0.5mm.

(B) Wing-specific overexpression of an established hyperactive variant *PLCG1*^{D1165H} causes wing morphology phenotypes similar to, but more severe than that of *PLCG1*^{D1019G} or *PLCG1*^{D1165G}. Scale bars, 0.5mm.

Figure 6. *PLCG1* variants affect important residues

(A) 3D structure of full-length rat Plcg1 (PDB code: 6PBC; rat Plcg1 shares 96.9% amino acid identity with human PLCG1). The conserved protein domains are labeled with different colors. Two major intracellular interfaces are circled by dashed lines: 1-The hydrophobic ridge between the sPH domain and the catalytic core (X-box and Y-box); and 2-The interface between the cSH2 domain and the C2 domain. The three residues affected by the variants are indicated by yellow balls.

(B) Enlarged views of the Asp1019 residue within the autoinhibition interface between sPH domain and the Y box. The potential interactions with nearby residues are indicated. Notably, the Ser1021 residue is outside of the hydrophobic ridge and shows no predicted interaction with the residues in the sPH domain.

(C) Enlarged views of the Asp1165 residue within the autoinhibition interface between the cSH2 domain and the C2 domain. The potential interactions with nearby residues are indicated.

(D) Enlarged view of the His380 residue within the X-box catalytic domain, in proximity to the Ca^{2+} cofactor. Structural analysis was performed via UCSF Chimera [83].

The Undiagnosed Diseases Network Consortia

Carlos A. Bacino, Ashok Balasubramanyam, Lindsay C. Burrage, Hsiao-Tuan Chao, Ivan Chinn, Gary D. Clark, William J. Craigen, Hongzheng Dai, Lisa T. Emrick, Shamika Ketkar, Seema R. Lalani, Brendan H. Lee, Richard A. Lewis, Ronit Marom, James P. Orengo, Jennifer E. Posey, Lorraine Potocki, Jill A. Rosenfeld, Elaine Seto, Daryl A. Scott, Arjun Tarakad, Alyssa A. Tran, Tiphanie P. Vogel, Monika Weisz Hubshman, Kim Worley, Hugo J. Bellen, Michael F. Wangler, Shinya Yamamoto, Oguz Kanca, Christine M. Eng, Pengfei Liu, Patricia A. Ward, Edward Behrens, Marni Falk, Kelly Hassey, Kosuke Izumi, Gonench Kilich, Kathleen Sullivan, Adeline Vanderver, Zhe Zhang, Anna Raper, Vaidehi Jobanputra, Mohamad Mikati, Allyn McConkie-Rosell, Kelly Schoch, Vandana Shashi, Rebecca C. Spillmann, Queenie K.-G. Tan, Nicole M. Walley, Alan H. Beggs, Gerard T. Berry, Lauren C. Briere, Laurel A. Cobban, Matthew Coggins, Elizabeth L. Fieg, Frances High, Ingrid A. Holm, Susan Korrick, Joseph Loscalzo, Richard L. Maas, Calum A. MacRae, J. Carl Pallais, Deepak A. Rao, Lance H. Rodan, Edwin K. Silverman, Joan M. Stoler, David A. Sweetser, Melissa Walker, Jessica Douglas, Emily Glanton, Shilpa N. Kobren, Isaac S. Kohane, Kimberly LeBlanc, Audrey Stephannie C. Maghiro, Rachel Mahoney, Alexa T. McCray, Amelia L. M. Tan, Surendra Dasari, Brendan C. Lanpher, Ian R. Lanza, Eva Morava, Devin Oglesbee, Guney Bademci, Deborah Barbouth, Stephanie Bivona, Nicholas Borja, Joanna M. Gonzalez, Kumarie Latchman, LéShon Peart, Adriana Rebelo, Carson A. Smith, Mustafa Tekin, Willa Thorson, Stephan Zuchner, Herman Taylor, Heather A. Colley, Jyoti G. Dayal, Argenia L. Doss, David J. Eckstein, Sarah Hutchison, Donna M. Krasnewich, Laura A. Mamounas, Teri A. Manolio, Tiina K. Urv, Maria T. Acosta, Precilla D'Souza, Andrea Gropman, Ellen F. Macnamara, Valerie V. Maduro, John J. Mulvihill, Donna Novacic, Barbara N. Pusey Swerdzewski, Camilo Toro, Colleen E. Wahl, David R. Adams, Ben Afzali, Elizabeth A. Burke, Joie Davis, Margaret Delgado, Jiayu Fu, William A. Gahl, Neil Hanchard, Yan Huang, Wendy Introne, Orpa Jean-Marie, May Christine V. Malicdan, Marie Morimoto, Leoyklang Petcharet, Francis Rossignol, Marla Sabaii, Ben Solomon, Cynthia J. Tifft, Lynne A. Wolfe, Heidi Wood, Aimee Allworth, Michael Bamshad, Anita Beck, Jimmy Bennett, Elizabeth Blue, Peter

Byers, Sirisak Chanprasert, Michael Cunningham, Katrina Dipple, Daniel Doherty, Dawn Earl, Ian Glass, Anne Hing, Fuki M. Hisama, Martha Horike-Pyne, Gail P. Jarvik, Jeffrey Jarvik, Suman Jayadev, Emerald Kaitryn, Christina Lam, Danny Miller, Ghayda Mirzaa, Wendy Raskind, Elizabeth Rosenthal, Emily Shelkowitz, Sam Sheppeard, Andrew Stergachis, Virginia Sybert, Mark Wener, Tara Wenger, Raquel L. Alvarez, Gill Bejerano, Jonathan A. Bernstein, Devon Bonner, Terra R. Coakley, Paul G. Fisher, Page C. Goddard, Meghan C. Halley, Jason Hom, Jennefer N. Kohler, Elijah Kravets, Beth A. Martin, Shruti Marwaha, Chloe M. Reuter, Maura Ruzhnikov, Jacinda B. Sampson, Kevin S. Smith, Shirley Sutton, Holly K. Tabor, Rachel A. Ungar, Matthew T. Wheeler, Euan A. Ashley, William E. Byrd, Andrew B. Crouse, Matthew Might, Mariko Nakano-Okuno, Jordan Whitlock, Manish J. Butte, Rosario Corona, Esteban C. Dell'Angelica, Naghmeh Dorrani, Emilie D. Douine, Brent L. Fogel, Alden Huang, Deborah Krakow, Sandra K. Loo, Martin G. Martin, Julian A. Martínez-Agosto, Elisabeth McGee, Stanley F. Nelson, Shirley Nieves-Rodriguez, Jeanette C. Papp, Neil H. Parker, Genecee Renteria, Janet S. Sinsheimer, Jijun Wan, Justin Alvey, Ashley Andrews, Jim Bale, John Bohnsack, Lorenzo Botto, John Carey, Nicola Longo, Paolo Moretti, Laura Pace, Aaron Quinlan, Matt Velinder, Dave Viskochil, Gabor Marth, Pinar Bayrak-Toydemir, Rong Mao, Monte Westerfield, Anna Bican, Thomas Cassini, Brian Corner, Rizwan Hamid, Serena Neumann, John A. Phillips III, Lynette Rives, Amy K. Robertson, Kimberly Ezell, Joy D. Cogan, Nichole Hayes, Dana Kiley, Kathy Sisco, Jennifer Wambach, Daniel Wegner, Dustin Baldridge, F. Sessions Cole, Stephen Pak, Timothy Schedl, Jimann Shin, and Lilianna Solnica-Krezel.

References

1. Berridge MJ, Irvine RF. Inositol trisphosphate, a novel second messenger in cellular signal transduction. Nature. 1984;312(5992):315-321.
2. Exton JH. Regulation of phosphoinositide phospholipases by hormones, neurotransmitters, and other agonists linked to G proteins. Annu Rev Pharmacol Toxicol. 1996;36:481-509.
3. Balla T. Phosphoinositides: tiny lipids with giant impact on cell regulation. Physiol Rev. 2013;93(3):1019-1137.
4. Majerus PW, Connolly TM, Deckmyn H, et al. The metabolism of phosphoinositide-derived messenger molecules. Science. 1986;234(4783):1519-1526.
5. Nishizuka Y. Turnover of inositol phospholipids and signal transduction. Science. 1984;225(4668):1365-1370.
6. Hilgemann DW. Local PIP(2) signals: when, where, and how? Pflugers Arch. 2007;455(1):55-67.
7. Hilgemann DW, Feng S, Nasuhoglu C. The complex and intriguing lives of PIP2 with ion channels and transporters. Sci STKE. 2001;2001(111):re19.
8. Suh BC, Hille B. PIP2 is a necessary cofactor for ion channel function: how and why? Annu Rev Biophys. 2008;37:175-195.
9. Nishizuka Y. Intracellular signaling by hydrolysis of phospholipids and activation of protein kinase C. Science. 1992;258(5082):607-614.
10. Berridge MJ. Inositol trisphosphate and calcium signalling. Nature. 1993;361(6410):315-325.
11. Yang YR, Choi JH, Chang JS, et al. Diverse cellular and physiological roles of phospholipase C-gamma1. Adv Biol Regul. 2012;52(1):138-151.
12. Cocco L, Follo MY, Manzoli L, Suh PG. Phosphoinositide-specific phospholipase C in health and disease. J Lipid Res. 2015;56(10):1853-1860.
13. Gomes DA, de Miranda MC, Faria J, Rodrigues MA. The basis of nuclear phospholipase C in cell proliferation. Adv Biol Regul. 2021;82:100834.
14. Asano S, Maetani Y, Ago Y, Kanematsu T. Phospholipase C-related catalytically inactive protein enhances cisplatin-induced apoptotic cell death. Eur J Pharmacol. 2022;933:175273.
15. Suh PG, Park JI, Manzoli L, et al. Multiple roles of phosphoinositide-specific phospholipase C isozymes. BMB Rep. 2008;41(6):415-434.
16. Kadamur G, Ross EM. Mammalian phospholipase C. Annu Rev Physiol. 2013;75:127-154.
17. Katan M, Cockcroft S. Phospholipase C families: Common themes and versatility in physiology and pathology. Prog Lipid Res. 2020;80:101065.
18. Gresset A, Sondek J, Harden TK. The phospholipase C isozymes and their regulation. Subcell Biochem. 2012;58:61-94.
19. Gresset A, Hicks SN, Harden TK, Sondek J. Mechanism of phosphorylation-induced activation of phospholipase C-gamma isozymes. J Biol Chem. 2010;285(46):35836-35847.
20. Hajicek N, Keith NC, Siraliev-Perez E, et al. Structural basis for the activation of PLC-gamma isozymes by phosphorylation and cancer-associated mutations. Elife. 2019;8.
21. Nosbisch JL, Bear JE, Haugh JM. A kinetic model of phospholipase C-gamma1 linking structure-based insights to dynamics of enzyme autoinhibition and activation. J Biol Chem. 2022;298(5):101886.
22. Homma Y, Takenawa T, Emori Y, Sorimachi H, Suzuki K. Tissue- and cell type-specific expression of mRNAs for four types of inositol phospholipid-specific phospholipase C. Biochem Biophys Res Commun. 1989;164(1):406-412.
23. Regunathan J, Chen Y, Kutlesa S, et al. Differential and nonredundant roles of phospholipase Cgamma2 and phospholipase Cgamma1 in the terminal maturation of NK cells. J Immunol. 2006;177(8):5365-5376.

24. Yu P, Constien R, Dear N, et al. Autoimmunity and inflammation due to a gain-of-function mutation in phospholipase C gamma 2 that specifically increases external Ca2+ entry. Immunity. 2005;22(4):451-465.
25. Ombrello MJ, Remmers EF, Sun G, et al. Cold urticaria, immunodeficiency, and autoimmunity related to PLCG2 deletions. N Engl J Med. 2012;366(4):330-338.
26. Zhou Q, Lee GS, Brady J, et al. A hypermorphic missense mutation in PLCG2, encoding phospholipase Cgamma2, causes a dominantly inherited autoinflammatory disease with immunodeficiency. Am J Hum Genet. 2012;91(4):713-720.
27. Neves JF, Doffinger R, Barcena-Morales G, et al. Novel PLCG2 Mutation in a Patient With APLAID and Cutis Laxa. Front Immunol. 2018;9:2863.
28. Consortium G. Human genomics. The Genotype-Tissue Expression (GTEx) pilot analysis: multitissue gene regulation in humans. Science. 2015;348(6235):648-660.
29. Ji QS, Winnier GE, Niswender KD, et al. Essential role of the tyrosine kinase substrate phospholipase C-gamma1 in mammalian growth and development. Proc Natl Acad Sci U S A. 1997;94(7):2999-3003.
30. Liao HJ, Kume T, McKay C, Xu MJ, Ihle JN, Carpenter G. Absence of erythrogenesis and vasculogenesis in Plcg1-deficient mice. J Biol Chem. 2002;277(11):9335-9341.
31. Arteaga CL, Johnson MD, Todderud G, Coffey RJ, Carpenter G, Page DL. Elevated content of the tyrosine kinase substrate phospholipase C-gamma 1 in primary human breast carcinomas. Proc Natl Acad Sci U S A. 1991;88(23):10435-10439.
32. Noh DY, Lee YH, Kim SS, et al. Elevated content of phospholipase C-gamma 1 in colorectal cancer tissues. Cancer. 1994;73(1):36-41.
33. Xie Z, Chen Y, Liao EY, Jiang Y, Liu FY, Pennypacker SD. Phospholipase C-gamma1 is required for the epidermal growth factor receptor-induced squamous cell carcinoma cell mitogenesis. Biochem Biophys Res Commun. 2010;397(2):296-300.
34. Park JG, Lee YH, Kim SS, et al. Overexpression of phospholipase C-gamma 1 in familial adenomatous polyposis. Cancer Res. 1994;54(8):2240-2244.
35. Kunze K, Spieker T, Gamerdinger U, et al. A recurrent activating PLCG1 mutation in cardiac angiosarcomas increases apoptosis resistance and invasiveness of endothelial cells. Cancer Res. 2014;74(21):6173-6183.
36. Behjati S, Tarpey PS, Sheldon H, et al. Recurrent PTPRB and PLCG1 mutations in angiosarcoma. Nat Genet. 2014;46(4):376-379.
37. Vaque JP, Gomez-Lopez G, Monsalvez V, et al. PLCG1 mutations in cutaneous T-cell lymphomas. Blood. 2014;123(13):2034-2043.
38. Bischof J, Bjorklund M, Furger E, Schertel C, Taipale J, Basler K. A versatile platform for creating a comprehensive UAS-ORFeome library in Drosophila. Development. 2013;140(11):2434-2442.
39. Bischof J, Maeda RK, Hediger M, Karch F, Basler K. An optimized transgenesis system for Drosophila using germ-line-specific phiC31 integrases. Proc Natl Acad Sci U S A. 2007;104(9):3312-3317.
40. Venken KJ, He Y, Hoskins RA, Bellen HJ. P[acman]: a BAC transgenic platform for targeted insertion of large DNA fragments in D. melanogaster. Science. 2006;314(5806):1747-1751.
41. Madabattula ST, Strautman JC, Bysice AM, et al. Quantitative Analysis of Climbing Defects in a Drosophila Model of Neurodegenerative Disorders. J Vis Exp. 2015(100):e52741.
42. Lu S, Hernan R, Marcogliese PC, et al. Loss-of-function variants in TIAM1 are associated with developmental delay, intellectual disability, and seizures. Am J Hum Genet. 2022;109(4):571-586.
43. Ravenscroft TA, Janssens J, Lee PT, et al. Drosophila Voltage-Gated Sodium Channels Are Only Expressed in Active Neurons and Are Localized to Distal Axonal Initial Segment-like Domains. J Neurosci. 2020;40(42):7999-8024.

44. Schneider CA, Rasband WS, Eliceiri KW. NIH Image to ImageJ: 25 years of image analysis. Nat Methods. 2012;9(7):671-675.
45. Splinter K, Adams DR, Bacino CA, et al. Effect of Genetic Diagnosis on Patients with Previously Undiagnosed Disease. N Engl J Med. 2018;379(22):2131-2139.
46. Sobreira N, Schiettecatte F, Valle D, Hamosh A. GeneMatcher: a matching tool for connecting investigators with an interest in the same gene. Hum Mutat. 2015;36(10):928-930.
47. Lek M, Karczewski KJ, Minikel EV, et al. Analysis of protein-coding genetic variation in 60,706 humans. Nature. 2016;536(7616):285-291.
48. Karczewski KJ, Francioli LC, Tiao G, et al. The mutational constraint spectrum quantified from variation in 141,456 humans. Nature. 2020;581(7809):434-443.
49. Quinodoz M, Royer-Bertrand B, Cisarova K, Di Gioia SA, Superti-Furga A, Rivolta C. DOMINO: Using Machine Learning to Predict Genes Associated with Dominant Disorders. Am J Hum Genet. 2017;101(4):623-629.
50. Wang J, Al-Ouran R, Hu Y, et al. MARRVEL: Integration of Human and Model Organism Genetic Resources to Facilitate Functional Annotation of the Human Genome. Am J Hum Genet. 2017;100(6):843-853.
51. Hu Y, Comjean A, Rodiger J, et al. FlyRNAi.org-the database of the Drosophila RNAi screening center and transgenic RNAi project: 2021 update. Nucleic Acids Res. 2021;49(D1):D908-D915.
52. Thackeray JR, Gaines PC, Ebert P, Carlson JR. small wing encodes a phospholipase C-(gamma) that acts as a negative regulator of R7 development in Drosophila. Development. 1998;125(24):5033-5042.
53. Trivedi D, Cm V, Bisht K, et al. A genome engineering resource to uncover principles of cellular organization and tissue architecture by lipid signaling. Elife. 2020;9.
54. Lee PT, Zirin J, Kanca O, et al. A gene-specific T2A-GAL4 library for Drosophila. eLife. 2018;7.
55. Diao F, Ironfield H, Luan H, et al. Plug-and-play genetic access to drosophila cell types using exchangeable exon cassettes. Cell Rep. 2015;10(8):1410-1421.
56. Diao F, White BH. A novel approach for directing transgene expression in Drosophila: T2A-Gal4 in-frame fusion. Genetics. 2012;190(3):1139-1144.
57. Donnelly MLL, Luke G, Mehrotra A, et al. Analysis of the aphthovirus 2A/2B polyprotein 'cleavage' mechanism indicates not a proteolytic reaction, but a novel translational effect: a putative ribosomal 'skip'. J Gen Virol. 2001;82(Pt 5):1013-1025.
58. Pan X, Alvarez AN, Ma M, et al. Allelic strengths of encephalopathy-associated UBA5 variants correlate between in vivo and in vitro assays. medRxiv. 2023.
59. Huang Y, Lemire G, Briere LC, et al. The recurrent de novo c.2011C>T missense variant in MTSS2 causes syndromic intellectual disability. Am J Hum Genet. 2022;109(10):1923-1931.
60. Lu S, Ma M, Mao X, et al. De novo variants in FRMD5 are associated with developmental delay, intellectual disability, ataxia, and abnormalities of eye movement. Am J Hum Genet. 2022;109(10):1932-1943.
61. Ma M, Zhang X, Zheng Y, et al. The fly homolog of SUPT16H, a gene associated with neurodevelopmental disorders, is required in a cell-autonomous fashion for cell survival. Hum Mol Genet. 2023;32(6):984-997.
62. Huang Y, Ma M, Mao X, et al. Novel dominant and recessive variants in human ROBO1 cause distinct neurodevelopmental defects through different mechanisms. Hum Mol Genet. 2022;31(16):2751-2765.
63. Venken KJ, Popodi E, Holtzman SL, et al. A molecularly defined duplication set for the X chromosome of Drosophila melanogaster. Genetics. 2010;186(4):1111-1125.
64. Robinow S, White K. Characterization and spatial distribution of the ELAV protein during Drosophila melanogaster development. J Neurobiol. 1991;22(5):443-461.
65. Sepp KJ, Schulte J, Auld VJ. Peripheral glia direct axon guidance across the CNS/PNS transition zone. Dev Biol. 2001;238(1):47-63.

66. Fischer JA, Giniger E, Maniatis T, Ptashne M. GAL4 activates transcription in Drosophila. Nature. 1988;332(6167):853-856.
67. Nagarkar-Jaiswal S, Lee PT, Campbell ME, et al. A library of MiMICs allows tagging of genes and reversible, spatial and temporal knockdown of proteins in Drosophila. Elife. 2015;4.
68. Blair SS. Wing vein patterning in Drosophila and the analysis of intercellular signaling. Annu Rev Cell Dev Biol. 2007;23:293-319.
69. Ross J, Kuzin A, Brody T, Odenwald WF. cis-regulatory analysis of the Drosophila pdm locus reveals a diversity of neural enhancers. BMC Genomics. 2015;16(1):700.
70. Kataoka K, Nagata Y, Kitanaka A, et al. Integrated molecular analysis of adult T cell leukemia/lymphoma. Nat Genet. 2015;47(11):1304-1315.
71. Siraliev-Perez E, Stariha JTB, Hoffmann RM, et al. Dynamics of allosteric regulation of the phospholipase C-gamma isozymes upon recruitment to membranes. Elife. 2022;11.
72. Tao P, Han X, Wang Q, et al. A gain-of-function variation in PLCG1 causes a new immune dysregulation disease. J Allergy Clin Immunol. 2023;152(5):1292-1302.
73. Liu Y, Bunney TD, Khosa S, et al. Structural insights and activating mutations in diverse pathologies define mechanisms of deregulation for phospholipase C gamma enzymes. EBioMedicine. 2020;51:102607.
74. Le Huray KIP, Bunney TD, Pinotsis N, Kalli AC, Katan M. Characterization of the membrane interactions of phospholipase Cgamma reveals key features of the active enzyme. Sci Adv. 2022;8(25):eabp9688.
75. Ellis MV, James SR, Perisic O, Downes CP, Williams RL, Katan M. Catalytic domain of phosphoinositide-specific phospholipase C (PLC). Mutational analysis of residues within the active site and hydrophobic ridge of plcdelta1. J Biol Chem. 1998;273(19):11650-11659.
76. Hajicek N, Charpentier TH, Rush JR, Harden TK, Sondek J. Autoinhibition and phosphorylation-induced activation of phospholipase C-gamma isozymes. Biochemistry. 2013;52(28):4810-4819.
77. Manso R, Rodriguez-Pinilla SM, Gonzalez-Rincon J, et al. Recurrent presence of the PLCG1 S345F mutation in nodal peripheral T-cell lymphomas. Haematologica. 2015;100(1):e25-27.
78. DeBell K, Graham L, Reischl I, Serrano C, Bonvini E, Rellahan B. Intramolecular regulation of phospholipase C-gamma1 by its C-terminal Src homology 2 domain. Mol Cell Biol. 2007;27(3):854-863.
79. Smith MR, Liu YL, Matthews NT, Rhee SG, Sung WK, Kung HF. Phospholipase C-gamma 1 can induce DNA synthesis by a mechanism independent of its lipase activity. Proc Natl Acad Sci U S A. 1994;91(14):6554-6558.
80. Wada J, Rathnayake U, Jenkins LM, et al. In vitro reconstitution reveals cooperative mechanisms of adapter protein-mediated activation of phospholipase C-gamma1 in T cells. J Biol Chem. 2022;298(3):101680.
81. Thakur S, Sinhari A, Jain P, Jadhav HR. A perspective on oligonucleotide therapy: Approaches to patient customization. Front Pharmacol. 2022;13:1006304.
82. Khvorova A, Watts JK. The chemical evolution of oligonucleotide therapies of clinical utility. Nat Biotechnol. 2017;35(3):238-248.
83. Pettersen EF, Goddard TD, Huang CC, et al. UCSF Chimera--a visualization system for exploratory research and analysis. J Comput Chem. 2004;25(13):1605-1612.
84. Bayram Y, Karaca E, Coban Akdemir Z, et al. Molecular etiology of arthrogryposis in multiple families of mostly Turkish origin. J Clin Invest. 2016;126(2):762-778.
85. Ebrazeh M, Ezzatifar F, Torkamandi S, et al. Association of the genetic variants in the endoplasmic reticulum aminopeptidase 2 gene with ankylosing spondylitis susceptibility. Int J Rheum Dis. 2021;24(4):567-581.
86. Franke A, McGovern DP, Barrett JC, et al. Genome-wide meta-analysis increases to 71 the number of confirmed Crohn's disease susceptibility loci. Nat Genet. 2010;42(12):1118-1125.

87. International Genetics of Ankylosing Spondylitis C, Cortes A, Hadler J, et al. Identification of multiple risk variants for ankylosing spondylitis through high-density genotyping of immune-related loci. Nat Genet. 2013;45(7):730-738.
88. Oleari R, Andre V, Lettieri A, et al. A Novel SEMA3G Mutation in Two Siblings Affected by Syndromic GnRH Deficiency. Neuroendocrinology. 2021;111(5):421-441.
89. Dalal D, Molin LH, Piccini J, et al. Clinical features of arrhythmogenic right ventricular dysplasia/cardiomyopathy associated with mutations in plakophilin-2. Circulation. 2006;113(13):1641-1649.
90. Gerull B, Heuser A, Wichter T, et al. Mutations in the desmosomal protein plakophilin-2 are common in arrhythmogenic right ventricular cardiomyopathy. Nat Genet. 2004;36(11):1162-1164.
91. Hakui H, Kioka H, Sera F, et al. Refractory Ventricular Arrhythmias in a Patient With Dilated Cardiomyopathy Caused by a Nonsense Mutation in BAG5. Circ J. 2022;86(12):2043.

Figure 1. The *PLCG1* homolog, *sl*, is conserved in *Drosophila*

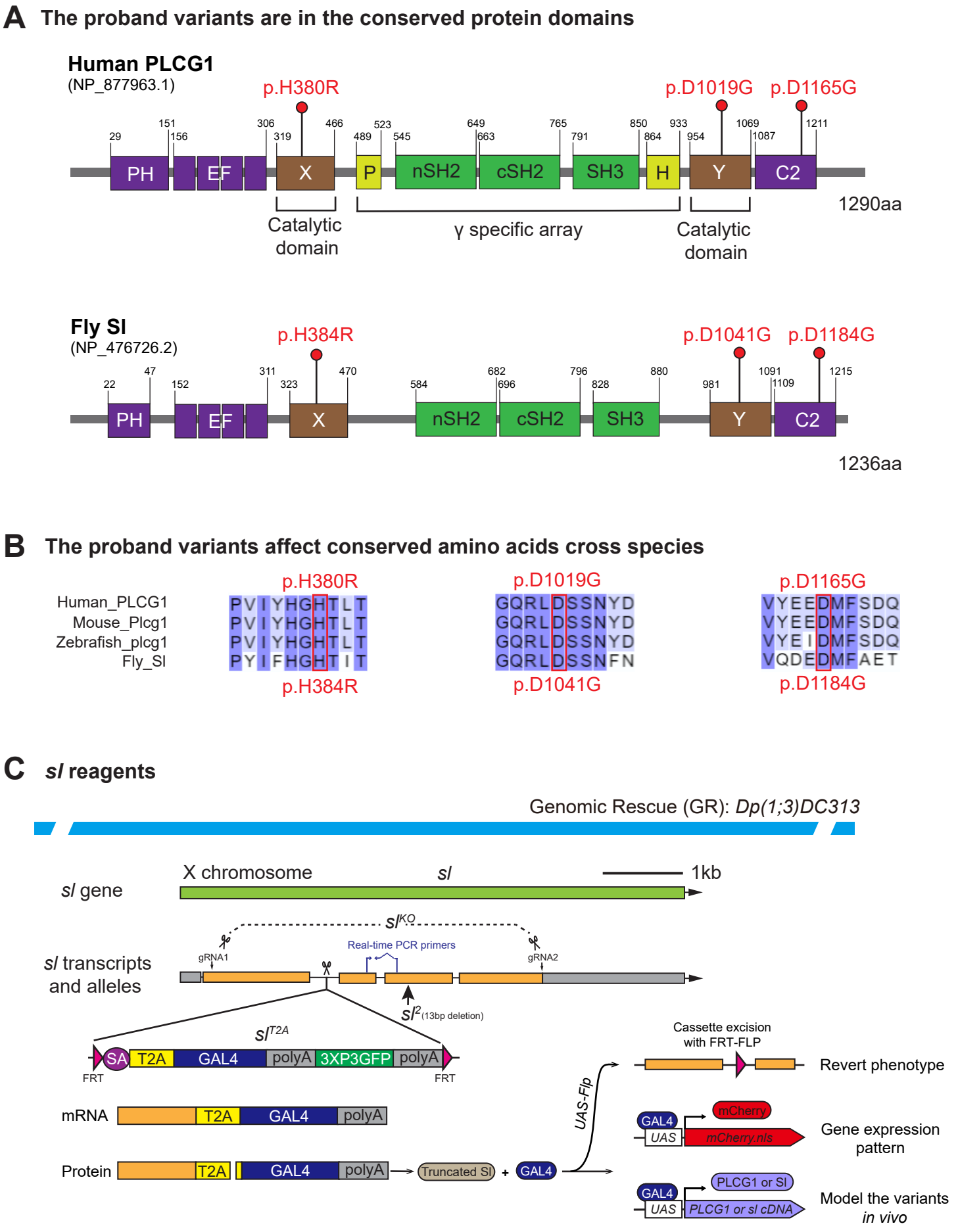

Figure 2. sl^{T2A} is a loss-of-function allele causing phenotypes in the wing and eye

A ***sl* is expressed in the developing wing and eye discs**

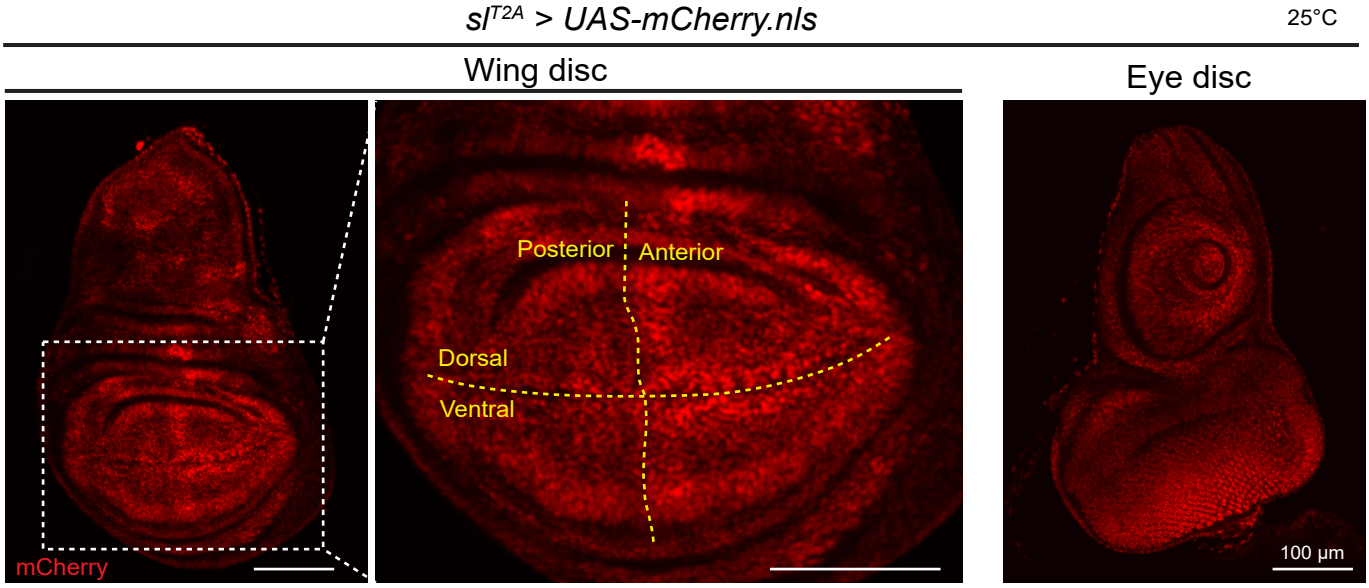

B ***sl*^{T2A} causes ectopic veins and reduction in the size of the adult wings**

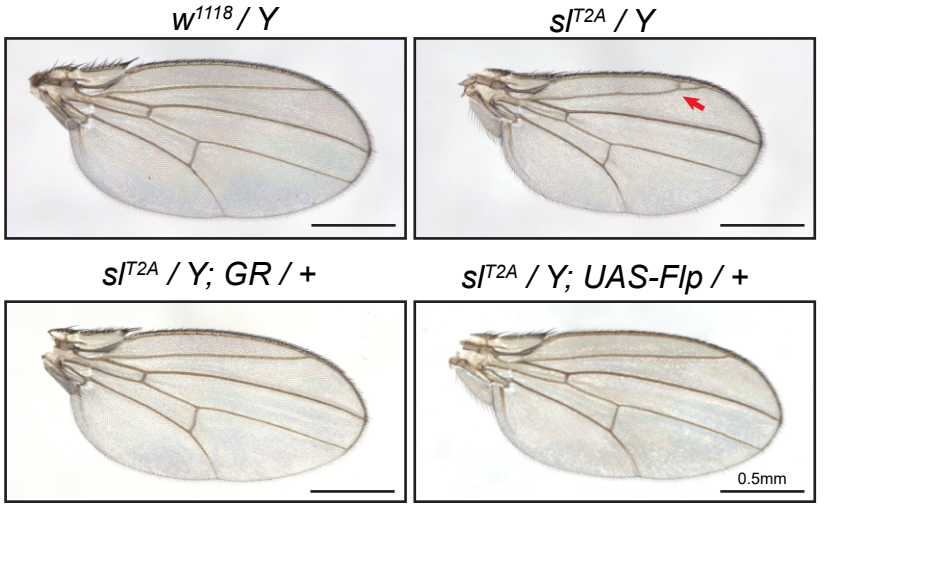

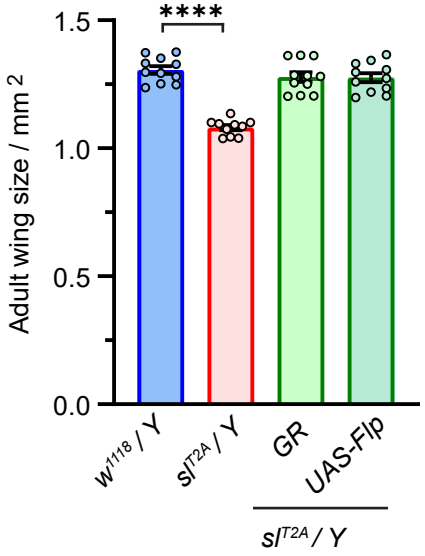

C ***sl*^{T2A} causes extra R7 photoreceptors in the adult eyes**

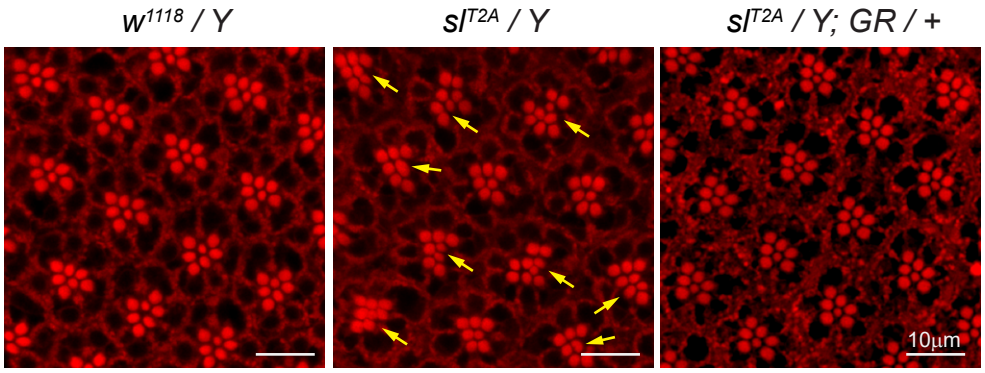

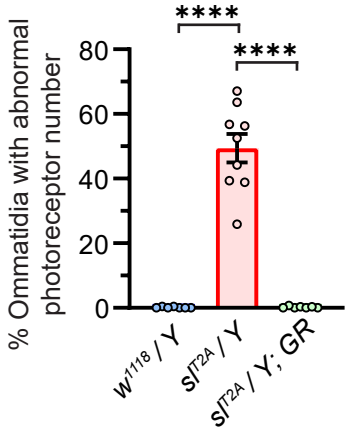

Figure 3. *sl* is expressed in a subset of neurons and glia in the CNS and loss of *sl* causes behavioral defects

A *sl* is expressed in the CNS in a subset of neurons and glia

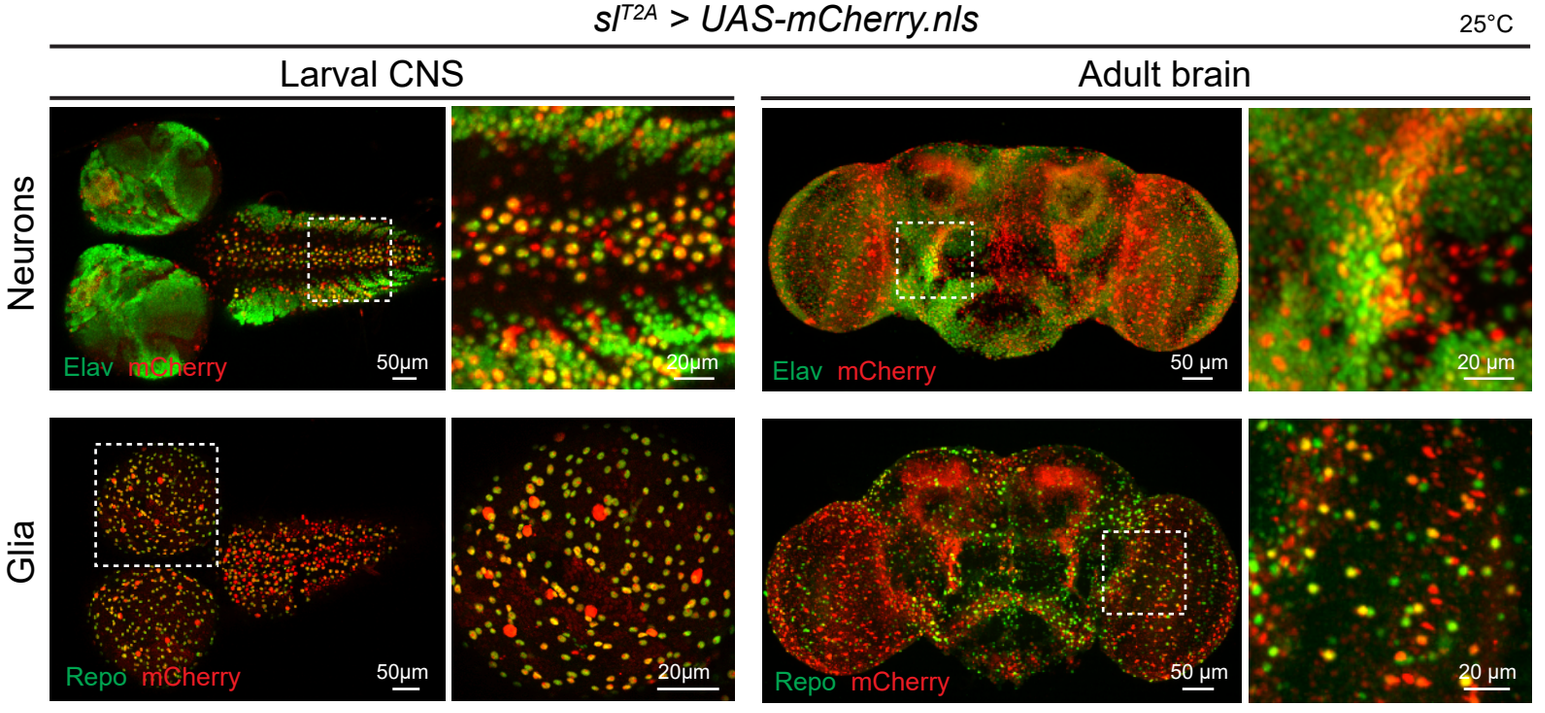

B Loss of *sl* causes behavioral defects including reduced lifespan and locomotor defect

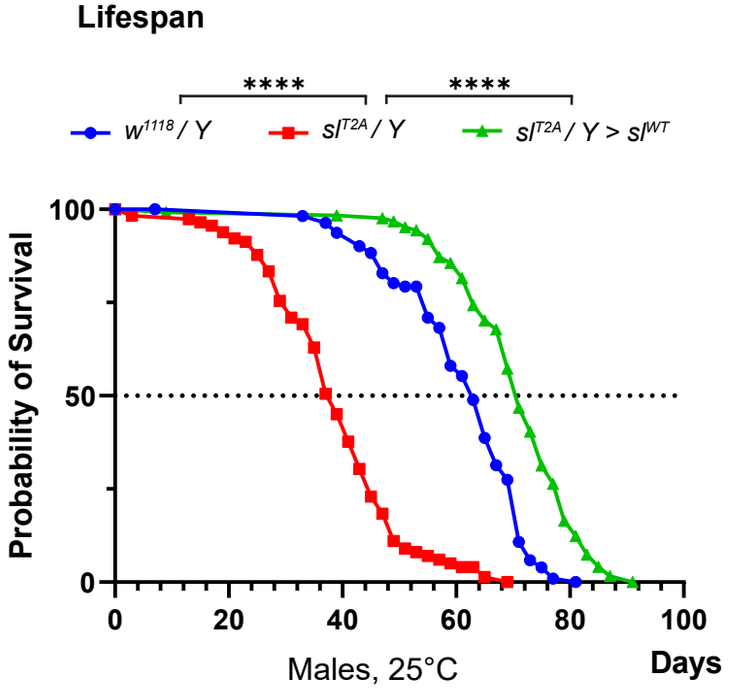

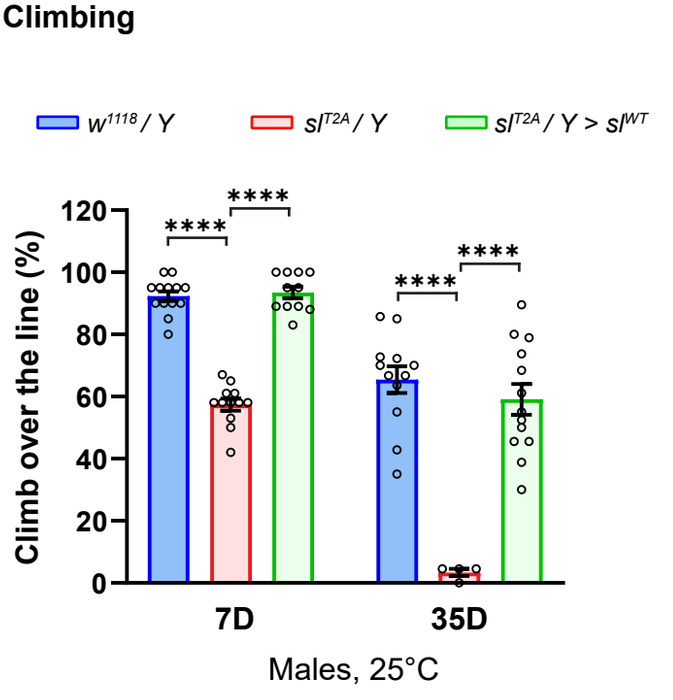

Figure 4. The variant cDNAs are toxic

A Expression of *UAS-sl* or *UAS-PLCG1* cDNAs in sl^{T2A} mutant flies

Cross Strategy

sl^{T2A} / *Balancer*
x
y w / Y; UAS-cDNA (or +)

↓

Progeny

sl^{T2A} / *y w*
sl^{T2A} / Y
Balancer / Y
Balancer / y w

; *UAS-cDNA* (or +) / +

Expected Mendelian Ratio
for each genotype is 0.25

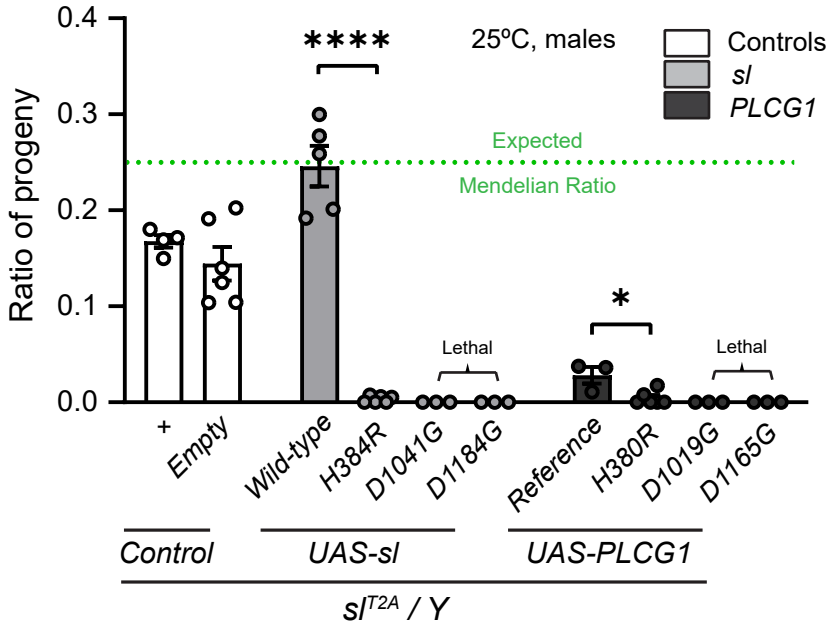

B Ubiquitous overexpression of *UAS-sl* or *UAS-PLCG1* using *Tub-GAL4*

Tub-GAl4 > UAS-sl cDNA 29ºC

Wild-type	*H384R*	*D1041G*	*D1184G*
Viable	Semi-lethal (~36% lethal)	L1-L2 lethal	L1-L2 lethal

Tub-GAl4 > UAS-PLCG1 cDNA 29ºC

Reference	*H380R*	*D1019G*	*D1165G*
Semi-lethal (~63% lethal)	Semi-lethal (~62% lethal)	L1-L2 lethal	L1-L2 lethal

C The toxicity caused by overexpressing human *PLCG1* cDNA is dosage sensitive

Tub-GAl4 > $PLCG1^{Reference}$

Expression level	
29°C	Semi-lethal (~63% lethal)
25°C	Semi-lethal (~43% lethal)
22°C	Viable

da-GAl4 > UAS-PLCG1 cDNA

Expression level	*Reference*	*D1019G*	*D1165G*	*H380R*
29°C	Viable	L1-L2 lethal	L1-L2 lethal	Viable
25°C	Viable	Semi-lethal (~80% lethal)	Semi-lethal (~84% lethal)	Viable
22°C	Viable	Viable	Viable	Viable

Figure 5. The *PLCG1* p.Asp1019Gly and p.Asp1165Gly variants are likely to be gain-of-function alleles

A **Wing-specific overexpression of *PLCG1*^{D1019G}, *PLCG1*^{D1165G} or their corresponding fly variants severely affect wing morphology**

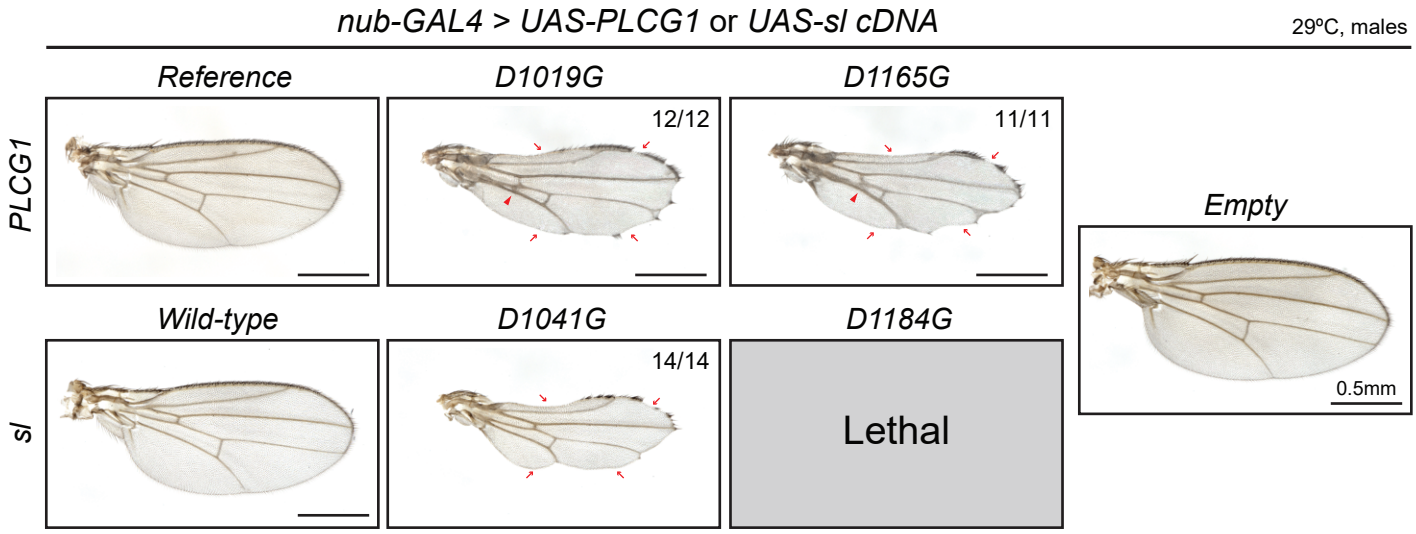

B **Comparison between the established somatic hyperactive *PLCG1*^{D1165H} and the genetic *PLCG1*^{D1019G}, *PLCG1*^{D1165G} variants**

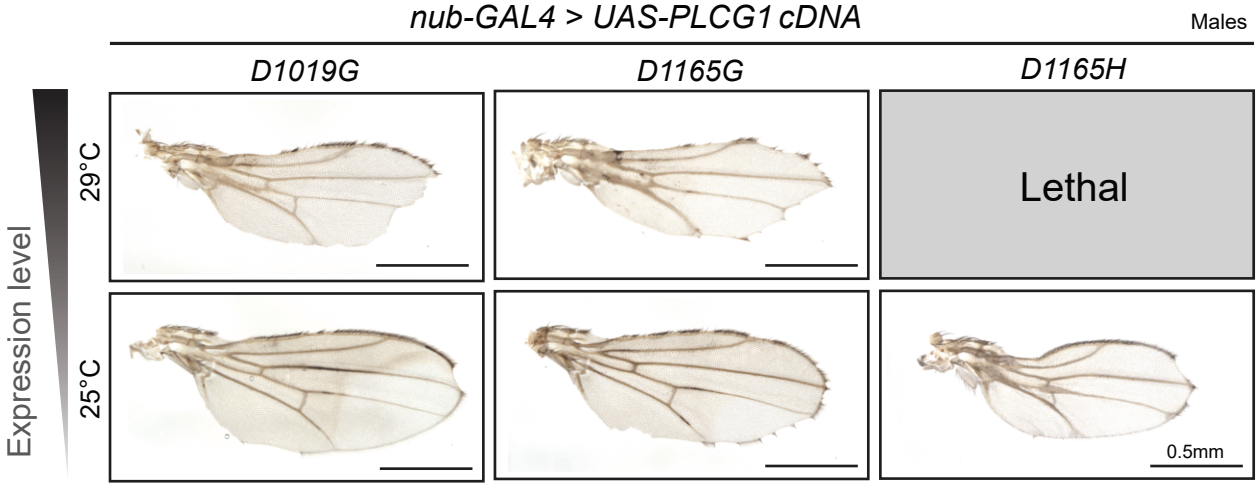

Figure 6. *PLCG1* variants affect important residues

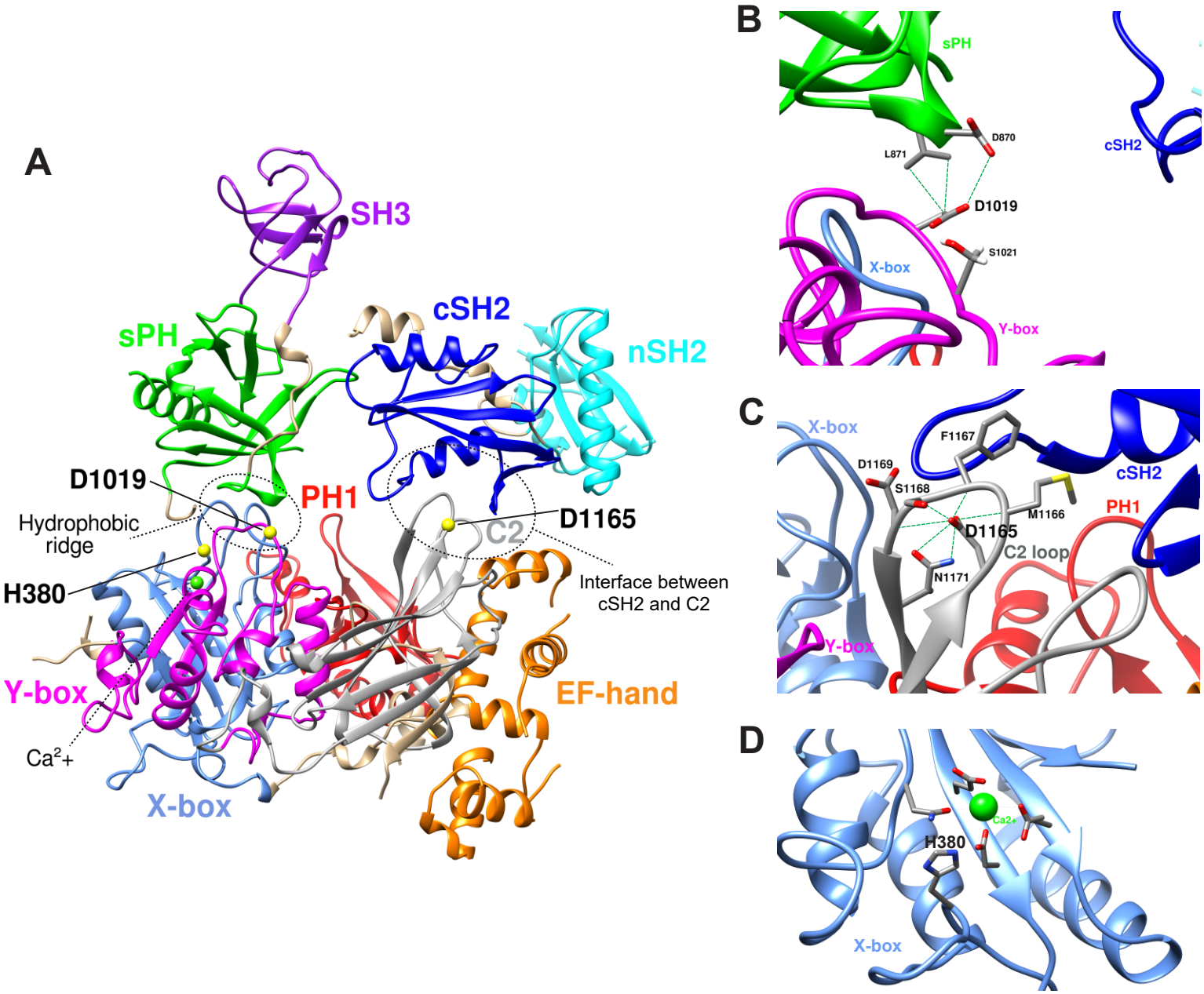

Supplemental Data

Additional variants identified in the probands

Proband 1 carries an intragenic duplication in *PSD3*. *PSD3* has not been associated with a Mendelian disorder but is potentially associated with an autosomal dominant arthrogryposis [1]. Hence, it may underlie the joint defects observed in proband 1.

Proband 2 has compound heterozygous missense variants in *ERAP2* and *SEMA3G*. *ERAP2* [MIM: 609497] has not been associated with a Mendelian disorder. It encodes an ER-residential metalloaminopeptidase that functions in the major histocompatibility class I antigen presentation pathway. Some variants in *ERAP2* are associated with a susceptibility to autoimmune diseases such as ankylosing spondylitis and Crohn's disease [2-4]. Given that proband 2 exhibits neuroinflammation and encephalitis, these phenotypes may be associated with the *ERAP2* variants. *SEMA3G* (Semaphorin 3G) has not been associated with a Mendelian disorder. However, a homozygous missense variant in *SEMAG3* was observed in two affected siblings from a consanguineous family. The siblings exhibited dysmorphic features as well as developmental delay [5].

Proband 3 carries a *de novo* missense variant in *PKP2* [MIM: 602861]. *PKP2* encodes Pakophilin-2 and has been associated with dominant arrhythmogenic right ventricular dysplasia 9 [MIM: 609040] [6-8]. However, this proband was born with septal defects.

Expression of human *PLCG1* reduces the viability of sl^{T2A} hemizygotes, and $PLCG1^{Reference}$ shows no obvious rescue of the phenotypes in the wings and eyes caused by loss of *sl*

We assessed if human *PLCG1* could effectively serve as a functional substitute for fly *sl* and rescue the loss-of-function phenotypes observed in *sl* mutant flies. However, only a small fraction of the sl^{T2A}/Y mutant hemizygotes expressing $PLCG1^{Reference}$ can survive to adults (Figure 4A). In addition to the obvious toxicity, $PLCG1^{Reference}$ fails to rescue the phenotypes observed in the wings or eyes of the *sl* mutant flies (Figure S6), which is fully rescued by fly sl^{WT} (Figure 2). This suggests that despite their high DIOPT score, human *PLCG1* cannot fully substitute for fly *sl*. It is possible that during the course of

evolution, *PLCG1* has acquired more specialized functions. For example, an essential step for enzymatic activation of mammalian PLCγ is the binding of its nSH2 domain to specific phosphotyrosines on the RTKs through a specific binding motif [9]. However, Thackeray *et al.* found that the consensus motif is absent in the intracellular domain of the *Drosophila* EGF receptor homolog DER [10], one of the three RTKs in *Drosophila* which is required for wing vein differentiation and photoreceptor formation [11-13].

Supplemental Figures and Legends

Figure S1. sl^{T2A} is a loss-of-function allele causing wing and eye phenotypes

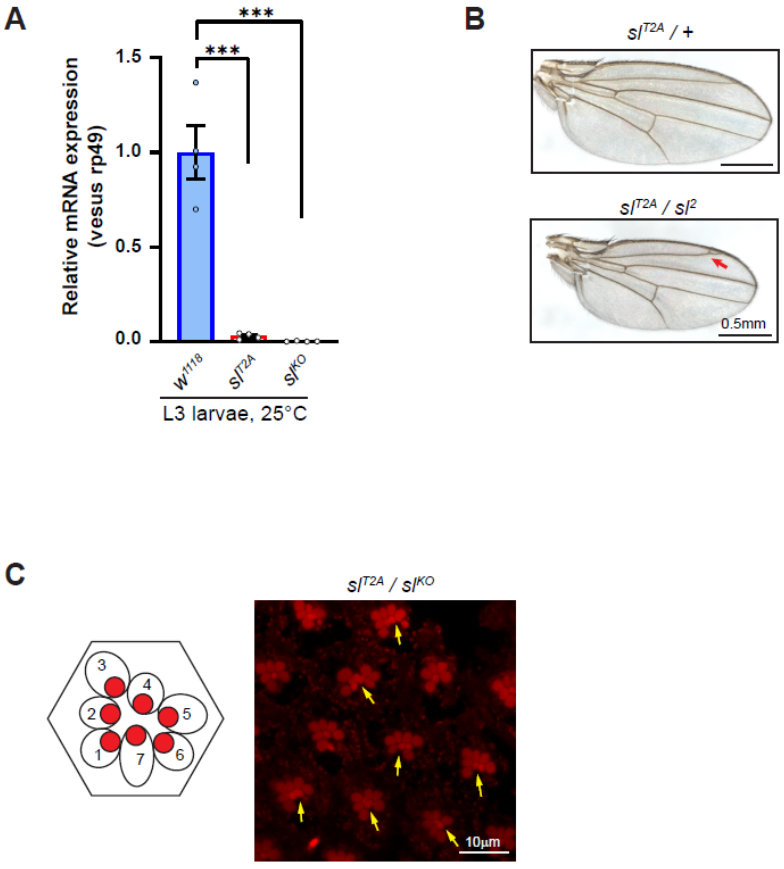

(A) Relative *sl* mRNA expression are <5% and <1% in sl^{T2A} and sl^{KO} mutant larvae when compared to controls (w^{1118}). The primers used for real-time PCR are shown in Figure 2A. Each dot represents a replicate per genotype. Unpaired t test, ***p<0.001.

(B) Representative images showing that sl^{T2A}/sl^{2} trans-heterozygous mutant flies have smaller wing and ectopic veins (indicated by arrow). Scale bars, 0.5mm.

(C) Representative images showing that sl^{T2A}/sl^{KO} trans-heterozygous mutant flies have extra photoreceptors (indicated by arrows). The schematic of the section of an ommatidia presenting seven photoreceptors (the R8 photoreceptor is not visible in such section) is shown. The photoreceptor rhabdomeres stain positive for phalloidin labeling F-actin. Scale bar, 10μm.

Figure S2. Ubiquitous overexpressing of *PLCG1*^{D1019G} or *PLCG1*^{D1165G} driven by *da-GAL4* causes pupal size reduction

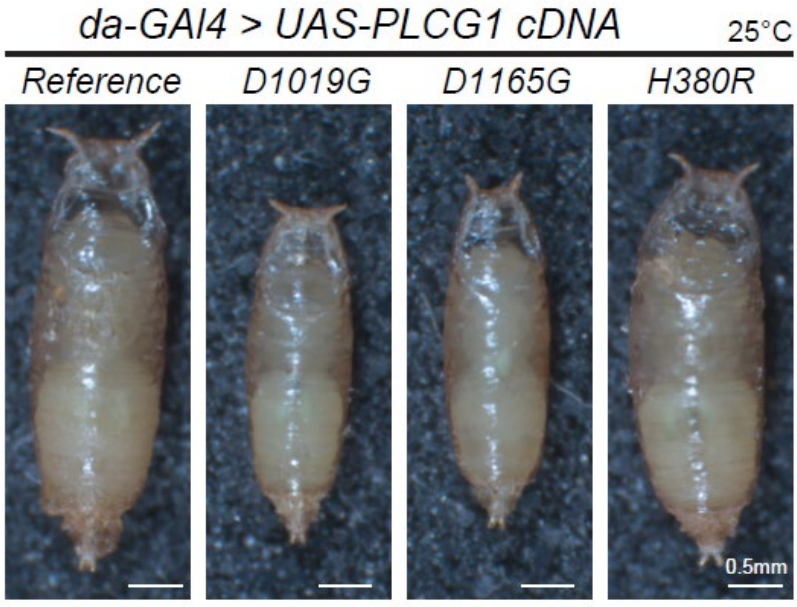

Representative images showing the pupal size of animals overexpressing *PLCG1* cDNAs by *da-GAL4* at 25°C. Overexpression of *PLCG1*^{D1019G} or *PLCG1*^{D1165G} causes pupae size reductions when compared to *PLCG1*^{Reference}. Overexpression of *PLCG1*^{H380R} is indistinguishable from *PLCG1*^{Reference}. Scale bars, 0.5mm.

Figure S3. Wing-specific overexpression of *PLCG1*^{Reference} or *sl*^{WT} causes wing size reduction, while overexpressing the *PLCG1*^{H380R} or *sl*^{H384R} further reduces wing size

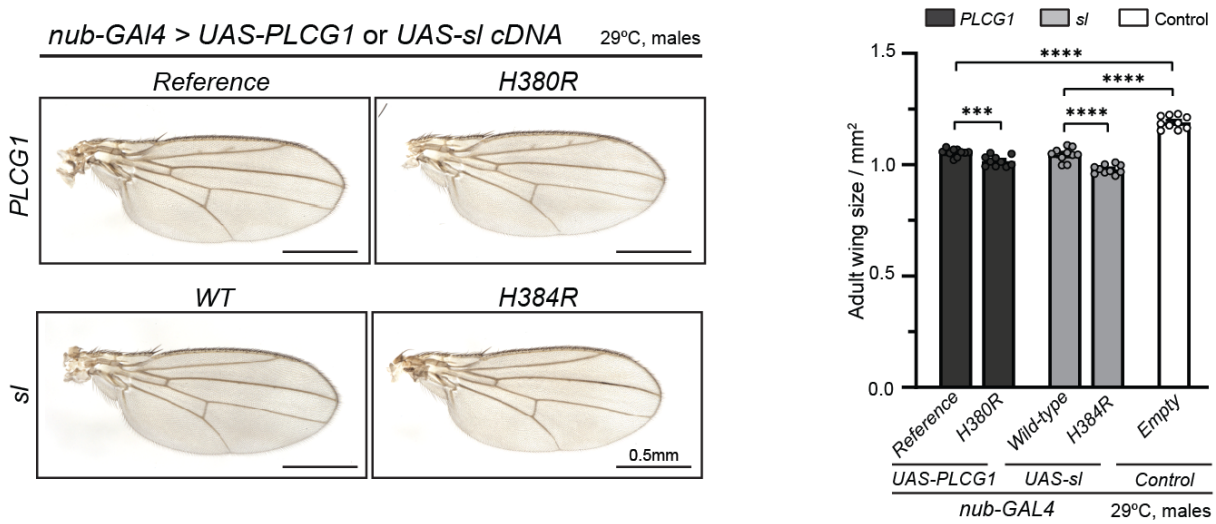

Representative images showing that wing-specific overexpression of *PLCG1*^{Reference} or *sl*^{WT} causes ~15% wing size reduction compared to the *UAS-Empty* control construct. Overexpression of *PLCG1*^{H380R} or *sl*^{H384R} causes a further ~5% size reduction. Each dot represents one measured adult wing. Unpaired t test, ***p<0.001, ****p < 0.0001, mean ± SEM. Scale bars, 0.5mm

Figure S4. Eye-specific overexpression of human *PLCG1* leads to size reduction in the eyes, and expression of the *PLCG1*^{D1019G} or *PLCG1*^{D1165G} causes more severe phenotype than expression of *PLCG1*^{Reference} or *PLCG1*^{H380R}

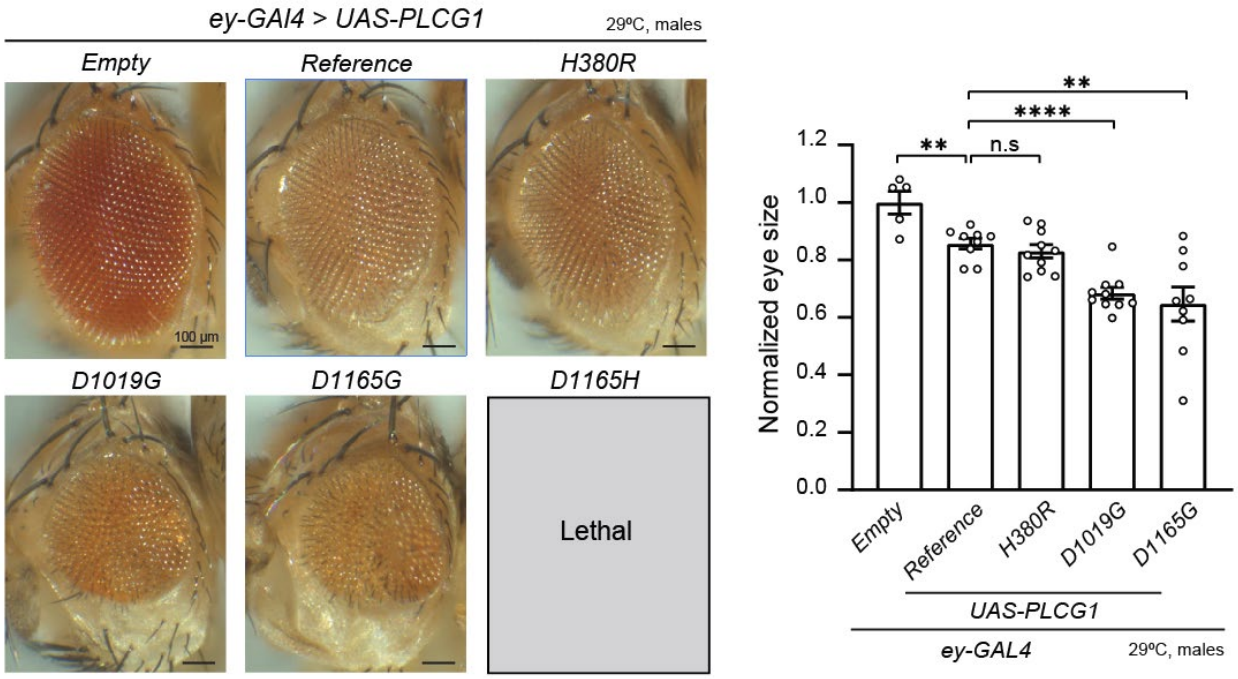

Representative images showing that eye-specific overexpression of *PLCG1*^{Reference} or *PLCG1*^{H380R} causes ~15% eye size reduction compared to the *UAS-Empty* control construct, whereas overexpression of *PLCG1*^{D1019G} or *PLCG1*^{D1165G} causes a ~30% size reduction. Overexpression of *PLCG1*^{D1165H} causes lethality. Each dot represents one measured adult eye. Unpaired t test, **p<0.01, ****p < 0.0001, ns: not significant, mean ± SEM. Scale bars, 100µm.

Figure S5. Ectopic expression of *PLCG1*^{S1021F} causes indistinguishable phenotypes in the wings or eyes compared to *PLCG1*^{Reference}

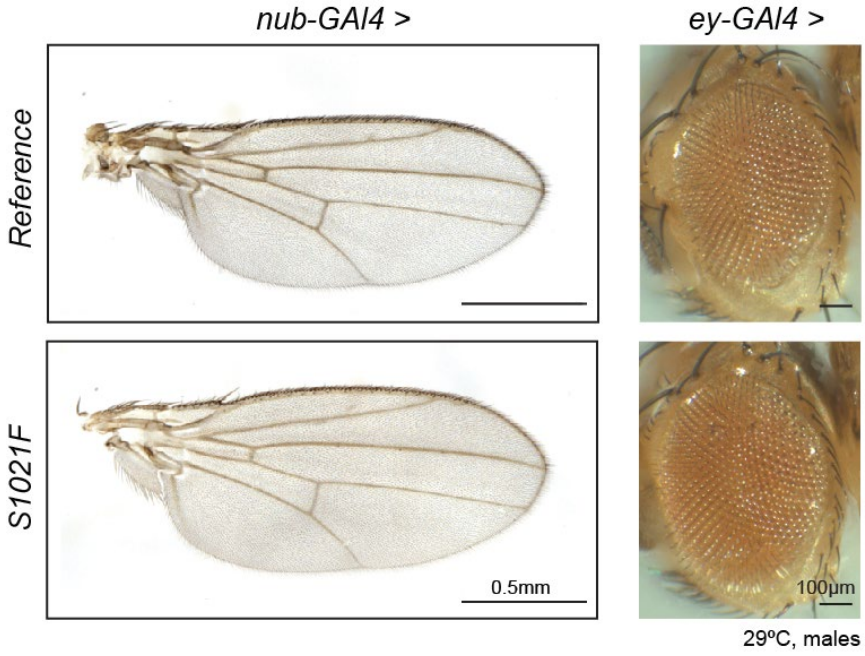

Representative images showing the adult wings and eyes with *PLCG1*^{S1021F} overexpression using *nub-GAL4* or *ey-GAL4*, respectively. There is no obvious morphological difference compared to *PLCG1*^{Reference}. Scale bars, 0.5mm in the wing images, 100μm in the eye images.

Figure S6. Expressing human *PLCG1* does not rescue wing and eye phenotypes associated with *sl*^{T2A}

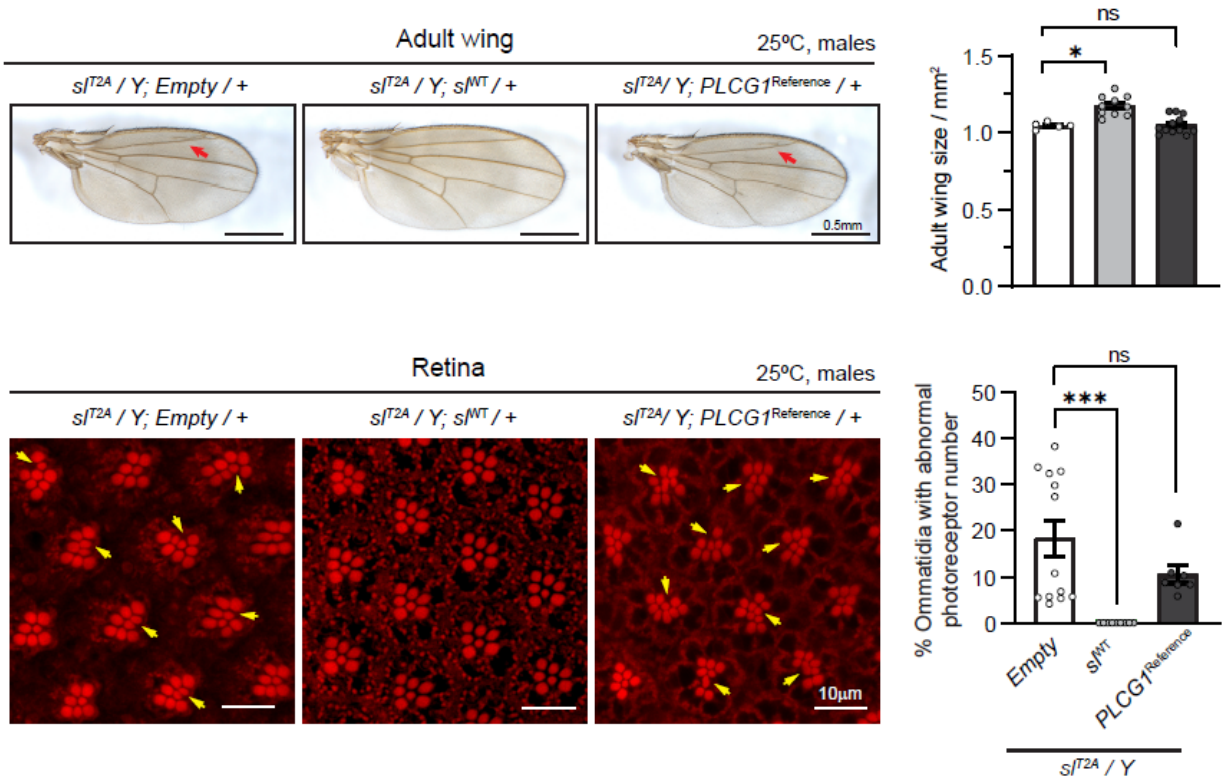

Representative images showing the adult wings (upper panel) and the photoreceptors (lower panel) expressing *PLCG1*^{Reference} or *sl*^{WT}. Expression of *sl*^{WT} rescues the loss-of-function phenotypes including wing size reduction, ectopic veins (indicated by red arrows) and extra photoreceptors (indicated by yellow arrows), whereas expression of the *PLCG1*^{Reference} or *UAS-Empty* shows no rescue. Scale bars, 0.5mm for the wing images and 10µm for the photoreceptor images. The photoreceptor rhabdomeres stain positive for phalloidin labeling F-actin. Quantification of the wing size (upper right panel) and the photoreceptors (lower right panel) are shown. Each dot represents one wing or one retina sample, respectively. Unpaired t test, ***p<0.001, *p<0.05. ns: not significant.

Supplemental Tables

Table S1. Pathogenicity prediction of the proband variants

Table S2. Mammalian PLC coding genes and their fly orthologs

Table S3. Fly strains used in the experiments

Table S4. Primers used in the experiments

Material and methods

Recruitment of the probands

Formal consents for genetic testing and publication were obtained from all probands or their family members. Probands 1 and 2 were recruited through the Undiagnosed Diseases Network (UDN) and were evaluated through the clinical research protocol of the National Institutes of Health Undiagnosed Diseases (15-HG-0130), which was approved by the National Human Genome Research Institute (NHGRI). Proband 3 was recruited through GeneMatcher.

Drosophila husbandry and generation of transgenic flies

The fly strains used in this study (listed in Table S3) were generated in house or obtained from the Bloomington Drosophila Stock Center (BDSC). All the flies were raised and maintained on standard fly food at room temperature unless specified. The sl^{T2A} allele was outcrossed with w^{1118} to clean up the genetic background. The strains used in this study were listed in Supplemental Table S3.

To generate the *UAS-cDNA* transgenic lines, human *PLCG1* cDNA was obtained from Horizon Discovery (MHS6278-213246131, clone ID 9052656), and fly *sl* cDNA was obtained from *Drosophila* Genomics Resource Center (DGRC, RE62235). The coding sequence (CDS) of $PLCG1^{Reference}$ and sl^{WT} were amplified using iProof™ High-Fidelity DNA Polymerase Kit (BioRad, #1725301), purified using QIAEX II Gel Extraction Kit (QIAGEN, #20021), sub-cloned into the Gateway compatible entry vector pDONR223 by BP cloning (BP clonase II, Thermo Fisher Scientific, #11789020) and sequentially cloned

into the destination vector pGW-attB-HA by LR cloning (LR clonase II, Thermo Fisher Scientific, #11791100) [14]. The variants were generated by site-directed mutagenesis strategy using Q5 Hot Start High-Fidelity 2x Master Mix (NEB, #M0494S) and *DpnI* restriction enzyme (NEB, # R0176L). All the constructs were sanger verified and injected, and inserted into the VK33 (*PBac{y[+]-attP}VK00033*) docking site using ϕC31 mediated transgenesis [15,16]. Primers are listed in Supplemental Table S4.

Drosophila behavioral assays

The climbing assay to examine the negative geotaxis and locomotion ability of the flies was performed as previously described [17,18] with some modifications. 18-22 flies per vial were transferred to an empty plastic vial and given 20min to rest prior to being tested. The flies were tapped to the bottom of the vial and were allowed to climb for 15s. The percentage of flies per vial that climbed over 5cm were calculated. The maximum distance from the bottom to the top is 18.5cm.

For the lifespan assay, newly eclosed male flies were collected and maintained at 25 °C (10 flies per vial). The flies were transferred to a new vial and the number of dead flies was counted every two days.

Immunostaining

Fly tissues were dissected in 1x PBS, fixed in 4% paraformaldehyde for 20min at room temperature, and washed in PBS (3 x 10min). For antibody staining, samples were treated with PBST (Triton X-100 in PBS, 0.1% for larval tissues, 2% for adult brain), 5% normal goat serum, and incubated in primary antibody overnight at 4°C. Samples were washed with 0.1% PBST (3 x 10min) and incubated with secondary antibody for 2h at room temperature (in darkness) and washed in 0.1% PBST (3 x 10min). Primary antibodies: rat anti-*Drosophila* Elav (1:250, DSHB, #7E8A10); mouse anti-*Drosophila* Repo (1:50, DSHB, #8D12). Secondary antibodies: goat anti-rat-647 (1:250, Jackson ImmunoResearch, #112-605-003), goat anti-mouse-Cy5 (1:250, Invitrogen, #A10524). Larval discs were mounted in Vectashield (Vector Labs #H1200 and #H1000). Larval CNS and adult brain were mounted in Rapiclear (Cedarlane,

#RC147001). For adult retinas, flies are reared at 25 °C under 12-h light/dark conditions. Retinas were isolated from 5-7 day old flies. Heads were dissected in PBS and fixed in 3.7% formaldehyde overnight at 4°C. The samples were rinsed with 0.1% PBST and the retinas were subsequently dissected and incubated with PBST-diluted phalloidin 647 (1:100, Invitrogen, #A22287) for 1h. Retinas were washed in 0.1% PBST and mounted in Vectashield. The images were obtained with a confocal microscope (Leica SP8X or Zeiss Airyscan LSM 880) and processed using the ImageJ-FIJI software [19].

Imaging of adult fly wings and eyes

To prepare the samples of adult fly wings, the wing blades were dissected and mounted in a glycerol/ethanol 1/1 mixture. Only wings from the same gender were compared to each other since females have larger wings than males when raised in the same conditions. To prepare the samples of adult fly eyes, the flies were frozen and placed onto a double-side stick tape with one eye facing up. The samples were imaged using bright field Stereomicroscope (Leica MZ16 or Leica Z16 APO). Image Pro Plus 7.0 software was used to for extended depth-of-field images. The image processing and the measurement of the total areas of the wing blades or eyes were conducted using the ImageJ-FIJI software [19].

Real-time PCR

Real-time PCR was performed as previously described [20] with modifications. All-In-One 5X RT MasterMix (abm, #G592), iTaq Universal SYBR Green Master Mix (BioRad#1725120) and BioRad C1000 Touch Cycler were used. Primers are listed in Supplemental Table S4.

Supplemental References

1. Bayram Y, Karaca E, Coban Akdemir Z, et al. Molecular etiology of arthrogryposis in multiple families of mostly Turkish origin. J Clin Invest. 2016;126(2):762-778.
2. Ebrazeh M, Ezzatifar F, Torkamandi S, et al. Association of the genetic variants in the endoplasmic reticulum aminopeptidase 2 gene with ankylosing spondylitis susceptibility. Int J Rheum Dis. 2021;24(4):567-581.
3. Franke A, McGovern DP, Barrett JC, et al. Genome-wide meta-analysis increases to 71 the number of confirmed Crohn's disease susceptibility loci. Nat Genet. 2010;42(12):1118-1125.
4. International Genetics of Ankylosing Spondylitis C, Cortes A, Hadler J, et al. Identification of multiple risk variants for ankylosing spondylitis through high-density genotyping of immune-related loci. Nat Genet. 2013;45(7):730-738.
5. Oleari R, Andre V, Lettieri A, et al. A Novel SEMA3G Mutation in Two Siblings Affected by Syndromic GnRH Deficiency. Neuroendocrinology. 2021;111(5):421-441.
6. Dalal D, Molin LH, Piccini J, et al. Clinical features of arrhythmogenic right ventricular dysplasia/cardiomyopathy associated with mutations in plakophilin-2. Circulation. 2006;113(13):1641-1649.
7. Gerull B, Heuser A, Wichter T, et al. Mutations in the desmosomal protein plakophilin-2 are common in arrhythmogenic right ventricular cardiomyopathy. Nat Genet. 2004;36(11):1162-1164.
8. Hakui H, Kioka H, Sera F, et al. Refractory Ventricular Arrhythmias in a Patient With Dilated Cardiomyopathy Caused by a Nonsense Mutation in BAG5. Circ J. 2022;86(12):2043.
9. Songyang Z, Shoelson SE, Chaudhuri M, et al. SH2 domains recognize specific phosphopeptide sequences. Cell. 1993;72(5):767-778.
10. Thackeray JR, Gaines PC, Ebert P, Carlson JR. small wing encodes a phospholipase C-(gamma) that acts as a negative regulator of R7 development in Drosophila. Development. 1998;125(24):5033-5042.
11. Dickson B, Hafen E. Genetics of signal transduction in invertebrates. Curr Opin Genet Dev. 1994;4(1):64-70.
12. Freeman M. Reiterative use of the EGF receptor triggers differentiation of all cell types in the Drosophila eye. Cell. 1996;87(4):651-660.
13. Schweitzer R, Shilo BZ. A thousand and one roles for the Drosophila EGF receptor. Trends Genet. 1997;13(5):191-196.
14. Bischof J, Bjorklund M, Furger E, Schertel C, Taipale J, Basler K. A versatile platform for creating a comprehensive UAS-ORFeome library in Drosophila. Development. 2013;140(11):2434-2442.
15. Bischof J, Maeda RK, Hediger M, Karch F, Basler K. An optimized transgenesis system for Drosophila using germ-line-specific phiC31 integrases. Proc Natl Acad Sci U S A. 2007;104(9):3312-3317.
16. Venken KJ, He Y, Hoskins RA, Bellen HJ. P[acman]: a BAC transgenic platform for targeted insertion of large DNA fragments in D. melanogaster. Science. 2006;314(5806):1747-1751.
17. Madabattula ST, Strautman JC, Bysice AM, et al. Quantitative Analysis of Climbing Defects in a Drosophila Model of Neurodegenerative Disorders. J Vis Exp. 2015(100):e52741.
18. Lu S, Hernan R, Marcogliese PC, et al. Loss-of-function variants in TIAM1 are associated with developmental delay, intellectual disability, and seizures. Am J Hum Genet. 2022;109(4):571-586.
19. Schneider CA, Rasband WS, Eliceiri KW. NIH Image to ImageJ: 25 years of image analysis. Nat Methods. 2012;9(7):671-675.
20. Ravenscroft TA, Janssens J, Lee PT, et al. Drosophila Voltage-Gated Sodium Channels Are Only Expressed in Active Neurons and Are Localized to Distal Axonal Initial Segment-like Domains. J Neurosci. 2020;40(42):7999-8024.